The immediate early protein 1 of human herpesvirus 6B counteracts ATM activation in an NBS1-dependent manner

Vanessa Collin[1,2,7], Élise Biquand[3,4,5,6,7], Vincent Tremblay[3,4,5,7], Élise G. Lavoie[3,5], Julien Dessapt[3,4,5], Andréanne Blondeau[3,5], Annie Gravel[1,2], Louis Flamand[1,2,*], Amélie Fradet-Turcotte[3,4,5,*]

[1] Division of Infectious Disease and Immunity, Centre Hospitalier Universitaire (CHU) de Québec-Université Laval Research Center, Quebec City, Quebec, Canada, G1V 4G2;

[2] Department of microbiology, infectious disease and immunology, Faculty of Medicine, Université Laval, Quebec City, Quebec, Canada, G1V 0A6;

[3] Oncology Division, Centre Hospitalier Universitaire (CHU) de Québec-Université Laval Research Center, Quebec City, Quebec, Canada, G1R 2J6;

[4] Department of Molecular biology, Medical Biochemistry and Pathology, Faculty of Medicine, Université Laval, Québec City, Quebec, Canada, G1V 0A6;

[5] Université Laval Cancer Research Center, Université Laval, Quebec City, Quebec, Canada, G1R 3S3;

[6] Current location: INSERM, Centre d'Étude des Pathologies Respiratoires (CEPR), UMR 1100, Université de Tours, Tours, France;

[7] These authors contributed equally to this work.

*Co-corresponding authors

Author Contributions: V.C., E.B., V.T., L.F., and A.F.-T. designed research; V.C., E.B., V.T., E.G.L., J.D., A.B., and A.G. performed research and analyzed data; V.C. and A.F.-T. wrote the original draft and E.B., V.T., and L.F. edited the manuscript.

Competing Interest Statement: The authors declare that they have no conflict of interest.

Classification: Biological sciences, Microbiology

Keywords: DNA double-strand break signaling, telomere; integration; human herpesvirus 6A/B; immediate-early protein IE1.

Co-corresponding authors' information:

Amélie Fradet-Turcotte

CRCHU de Québec Research center – Hotel-Dieu de Québec

9 McMahon, room 3744, Québec, Québec, Canada, G1R 2J6

Tel : 1-418-525-4444 x16473

amelie.fradet-turcotte@crchudequebec.ulaval.ca

Louis Flamand

CRCHU de Québec Research center – CHUL

2705 boulevard Laurier, T1-64, Québec, Québec, Canada G1V 4G2

Tel : 1-418-525-4444 x46164

louis.flamand@crchudequebec.ulaval.ca

Abstract

Viral infection often trigger an ATM-dependent DNA damage response (DDR) in host cells that suppresses viral replication. To counteract this antiviral surveillance system, viruses evolved different strategies to induce the degradation of the MRE11/RAD50/NBS1 (MRN) complex and prevent subsequent DDR signaling. Here, we report that human herpesvirus 6B (HHV-6B) infection causes genomic instability by suppressing the host cell's ability to induce ATM-dependent signaling pathways. Expression of immediate early protein 1 (IE1) phenocopies this phenotype and blocks further homology-directed double-strand break (DSB) repair. In contrast to other viruses, IE1 does not affect the stability of the MRN complex. Instead, it uses two distinct domains to inhibit ATM serine/threonine kinase (ATM) activation at DSBs. Structure-based analyses revealed that the N-terminal domain of IE1 interacts with the BRCA1 C-terminal domain 2 of nibrin (NBN, also known as NBS1), while ATM inhibition is attributable to on its C-terminal domain. Consistent with the role of the MRN complex in antiviral responses, NBS1 depletion resulted in increased HHV-6B replication in infected cells. However, in semi-permissive cells, viral integration of HHV-6B into the telomeres was not strictly dependent on NBS1, supporting models where this process occurs via telomere elongation rather than through DNA repair. Interestingly, as IE1 expression has been detected in cells of subjects with inherited chromosomally-integrated form of HHV-6B (iciHHV-6B), a condition associated with several health conditions, our results raise the possibility of a link between genomic instability and the development of iciHHV-6-associated diseases.

Significance Statement

Many viruses have evolved ways to inhibit DNA damage signaling, presumably to prevent infected cells from activating an antiviral response. Here, we show that this is also true for human herpesvirus 6B (HHV-6B), through its immediate early protein 1 (IE1). However, in contrast to adenovirus' immediate early proteins, HHV-6B IE1 is recruited to double-strand breaks in an NBS1-dependent manner and inhibits ATM serine/threonine kinase activation. Characterizing this phenotype revealed a unique mechanism by which HHV-6B manipulates DNA damage signaling in infected cells. Consistently, viral replication is restricted by the MRN complex in HHV-6B infected cells. Viral integration of HHV-6B into the host's telomeres is not strictly dependent on NBS1, challenging current models where integration occurs through homology-directed repair.

Introduction

To infect a cell, a virus needs to successfully replicate its genetic material and produce new virions. Accordingly, cells have a sophisticated surveillance system that detects viral DNA and activates an innate antiviral response. Mounting evidence supports a role for the DNA damage response (DDR) in this process, revealing an intricate interplay between its activation and the activation of intrinsic antiviral responses (1). Some viruses, such as adenovirus, target the MRE11-RAD50-NBS1 (MRN) complex for degradation to prevent the activation of ATM serine/threonine kinase (ATM) (2, 3), while others, such as herpes simplex virus 1 (HSV-1) and human papillomavirus, rely on these proteins for efficient viral replication (4–6). How and why viruses inhibit or hijack the ATM pathway remains a mystery (7).

In mammalian cells, the MRN complex and ATM are essential to maintain genomic stability in the presence of DNA double-strand breaks (DSBs). Broken DNA ends are first detected by the MRN complex (8), where its accumulation induces a signaling cascade that activates ATM and subsequent phosphorylation of the histone variant H2AX on Ser139 (producing γ-H2AX). Mediator of DNA damage checkpoint 1 (MDC1) interacts with γ-H2AX, triggering the ubiquitylation of chromatin surrounding the break by promoting the accumulation of the E3-ubiquitin ligases ring finger protein (RNF) 8 and RNF168 (9, 10). In the G1 phase of the cell cycle, the recruitment of the DNA repair factor tumor protein p53 binding protein 1 (53BP1) at ubiquitylated chromatin promotes DNA repair *via* non-homologous end-joining (NHEJ)(11). In the S and G2 phases, BRCA1 DNA repair associated (BRCA1) and RB binding protein 8 endonuclease (CtIP) accumulate at the break and cooperate with exonuclease 1 (EXO1), BLM RecQ like helicase, and DNA replication helicase/nuclease 2 (BLM-DNA2) to facilitate end resection. This process results in extensive single-stranded (ss) DNA accumulation, which ultimately triggers the recruitment of recombinases that drive the homology searching required for homology-driven recombination (HDR) (12). HDR uses homologous sequences as templates to repair breaks in a faithful manner and includes processes such as homologous recombination (HR), single-stranded annealing (SSA), and break-induced replication (BIR) (11, 13–15).

Human herpesvirus 6B (HHV-6B) is a betaherpesvirus that infects nearly 90% of the world's population in the first 2 years of life and is responsible for roseola infantum, a pathology defined by skin rashes, high fever, and respiratory distress (16–18). In this double-stranded DNA (dsDNA) virus subfamily, HHV-6B shares 90% homology with HHV-6A, another lymphotropic virus. Although both infect $CD4^+$ T lymphocytes, they have epidemiological, biological, and immunological differences (19). Like other herpesviruses, HHV-6A and HHV-6B (HHV-6A/B) establish lifelong latency in infected hosts and can occasionally reactivate (20). However, whereas most herpesviruses achieve latency by circularizing and silencing their genome, HHV-6A/B integrate their genomes into the host's chromosomal terminal repeats (telomeres) (21, 22). The linear dsDNA genomes of HHV-6A/B are both flanked by an array of direct repeats containing 15–180 reiterations of perfect telomeric repeats (pTMRs) identical to the human telomeric sequence (5′-TTAGGG-3′), enabling viral integration (23). This process depends on the integrity of these pTMRs (23), resulting in a model in which viral integration is mediated through HDR, including the SSA or BIR DNA repair mechanisms (24). When HHV-6A/B integration occurs in a gamete before fertilization, the newborn carries a copy of HHV-6A/B in every cell of its body and can be transmitted to its offspring. This condition, called inherited chromosomally-integrated (ici)HHV-6A/B, affects ~1% of the world's population, representing almost 80 million people (25, 26). It is more prevalent in

113 those suffering from health issues such as high spontaneous abortion rates (27, 28), pre-eclampsia (29), and
114 angina pectoris (30) compared to healthy subjects (reviewed in (31, 32)). However, the reason why iciHHV-
115 6A/B contributes to these clinical syndromes has not been elucidated in any detail.

116 HHV-6B, which is better characterized than HHV-6A, sequentially expresses more than 97
117 genes/proteins during its lytic cycle(33). Immediate early (IE) proteins are expressed early in the viral cycle, to
118 regulate viral gene expression and establish a favorable environment for viral replication. In the context of HHV-
119 6B, IE protein 1 (IE1) is the first protein expressed during cell infection (34). It inhibits the innate antiviral
120 response in part by sequestering signal transducer and activator of transcription 2 (STAT2) in the nucleus,
121 thereby compromising type I interferon production and signaling(35, 36). In infected cells, IE1 is exclusively
122 localized within PML bodies (37), which were recently implicated in HDR-mediated DNA repair through an
123 undefined mechanism (38–41). Interestingly, PML depletion reduces HHV-6B integration (42), suggesting that
124 IE1-containing PML bodies also participate in viral integration.

125 In this study, we report that HHV-6B infection—and more specifically, IE1 expression—leads to genomic
126 instability in cells. Further investigations revealed that IE1 specifically prevents phosphorylation of the histone
127 variant H2AX and subsequent HDR repair. Structure-function analyses reveal that IE1 interacts with NBS1 and
128 inhibits ATM. Consistent with a role for the MRN complex in interfering with viral replication, we show that NBS1
129 depletion results in increased HHV-6B replication in infected cells. Although current models propose that viral
130 integration occurs through HDR DNA repair, we show that viral integration is not affected in NBS1-depleted
131 cells that elongate their telomeres in a human telomerase reverse transcriptase (hTERT)-dependent manner
132 (42). Thus, our findings reveal that viral integration relies on biological pathways that safeguard telomere
133 extension in infected cells and not on specific DNA repair pathways.

134

135 **Results**

136 **HHV-6B infection and IE1 expression induce genomic instability**

137 Our first indication that HHV-6B infection induces genomic instability in host cells was the observation
138 that HHV-6B infection rapidly induced micronuclei (MNi) formation in MOLT-3 cells (a lymphoblast T cell line;
139 Fig.1*A* and *SI Appendix*, Fig. S1*A*). In these experiments, cells infected with the HHV-6B strain Z29 accumulated
140 6.6-fold more MNi than non-infected cells (Mock) 24 h post-infection (Fig.1*A*). Consistent with the rapid
141 accumulation of genomic instability in infected cells, we observed a similar phenotype in duplicate clones of
142 stable U2OS cell lines containing a doxycycline (Dox)-inducible expression cassette for IE1 (C10 and C102;
143 Fig. 1*B* and *SI Appendix*, Fig. S1*B*-*C*). These clones had 4.8-fold more MNi than parental U2OS cells 48 h post-
144 IE1 induction (Fig.1*B*), suggesting that the instability observed in HHV-6B infected cells is at least partially
145 caused by IE1. Note that both U2OS clone (C10 and C102) exhibit similar levels of MNi than the parental cell
146 line without IE1 induction (*SI Appendix*, Fig. S1*C*). MNi arise from unresolved genomic instabilities such as
147 DSBs (i), lagging chromosomes (ii), and ruptured anaphase bridges (ABs) (iii) (Fig. 1*C*) (43). They are
148 compartmentally separated from the primary nucleus and surrounded by a nuclear envelope, as shown by the
149 presence of lamin B in these perinuclear structures (*SI Appendix*, Fig. S1*D*-*E*) (44). To determine how IE1
150 triggers MNi formation, we analyzed the accumulation of different markers in IE1-induced MNi, such as

151 centromeres and telomeric DNA (to detect lagging chromosomes and ABs caused by telomere fusion,
152 respectively). Interestingly, a much lower proportion of the IE1-induced MNi contained centromeres compared
153 with those in parental U2OS cells (~10-fold, Fig. 1*D* and *SI Appendix*, Fig. S1*F*), suggesting that they are not
154 induced by chromosome segregation defects. Although IE1 partially colocalizes with telomeres in host cells
155 (42), fluorescence *in situ* hybridization (FISH) revealed that IE1 does not specifically promote instability at
156 telomeres, as IE1-induced MNi accumulated similar levels of telomeric DNA as those in parental U2OS cells
157 (Fig. 1*E* and *SI Appendix*, Fig. S1*G*). Metaphase spread assays revealed that IE1-expressing U2OS cell lines
158 exhibited higher frequencies of DNA breaks than parental cells (Fig. 1*F-G*), consistent with MNi being induced
159 by DSB accumulation. Interestingly, IE1 was detected in only 5–10% of the MNi (*SI Appendix*, Fig. S1*H*),
160 suggesting that they are not arising from DSBs induced by the physical binding of IE1 at any defined DNA locus.

161

162 **HHV-6B IE1 impairs DSB signaling and homology-directed DNA repair**

163 DSB accumulation results from either an increase in DNA breaks or defective DNA DSB signaling and
164 repair. To determine how HHV-6B infection promotes genomic instability, we first investigated whether infected
165 cells accumulated Ser139-phosphorylated H2AX (*i.e.*, the DSB marker γ-H2AX). Surprisingly, while γ-H2AX foci
166 accumulated in > 75% of non-infected MOLT-3 cells exposed to irradiation (IR), this number was dramatically
167 reduced in infected cells (Fig. 2*A-B* and *SI Appendix*, Fig. S2*A*). U2OS clones stably expressing IE1 reproduced
168 this phenotype (Fig. 2*C-D* and *SI Appendix*, Fig. S2*B*), indicating that IE1 impairs DSB signaling. This inhibition
169 is independent of IE1 accumulation within PML bodies, as no γ-H2AX foci were detected in PML-deficient U2OS
170 cells that transiently express IE1 (*PML*$^{-/-}$, Fig. 2*E* and *SI Appendix*, Fig. S2*C-E*).

171 DSB signaling is essential to activate DNA repair pathways. Therefore, we tested whether DNA repair
172 is inhibited in HHV-6B IE1-expressing cells. As mammalian cells use several pathways to repair DSBs (45), we
173 performed a panel of DNA repair reporter assays in cells with stable or transient IE1 expression. These reporter
174 assays all rely on the detection of a fluorescent protein that is expressed only if a site-specific DSB (induced by
175 either I-SceI or Cas-9) is adequately repaired (Fig. 3*A-D* and *SI Appendix*, Fig. S3*A*, top panels) (46, 47). In the
176 DR-GFP (direct repeats) and CRISPR-LMNA HDR assays, DSBs repaired by HR either reconstitute a defective
177 green fluorescent protein (GFP)-reporter transgene integrated into the genome (DR-GFP) or introduce a
178 cassette expressing mRuby in frame with endogenous lamin A (CRISPR-LMNA HDR), respectively (48, 49). In
179 SA-GFP (single-strand annealing), proper annealing of a small homologous stretch reconstitutes a truncated
180 GFP (48). In BIR-GFP (break-induced replication), replication-mediated repair following homology searching
181 places a GFP coding sequence in the correct orientation (15, 50). Finally, in NHEJ-GFP, the ends of two DSBs
182 need to be correctly ligated to recreate a full-length (FL) GFP-expressing cassette (51, 52). In assays using
183 reporter transgenes integrated into the genome (DR-GFP, SA-GFP, BIR-GFP, and NHEJ-GFP) (Fig. 3*A-D* and
184 *SI Appendix*, Fig. S3*B-C*), a condition without endonuclease I-SceI or Cas-9 was used as a negative control
185 and the percentage of fluorescent cells obtained with I-SceI was set to 1. In each condition, a small amount of
186 a near-infrared fluorescent protein (iRFP)-expressing vector was transfected with I-SceI, IE1, or an empty vector
187 (EV) to ensure that DNA repair was measured in transfected cells only, and DNA repair was assessed 48 or 72
188 h post-transfection. Finally, as the clonal BIR-GFP U2OS cell line was generated in this study using a previously
189 described BIR-GFP reporter plasmid(50), we used short interfering (si)RNAs against RAD51 and RAD52 as

190 additional controls (*SI Appendix*, Fig. S3*D-F*) (13). As expected, the BIR-GFP signal was specifically inhibited
191 in cells depleted of RAD51 (50).
192 Interestingly, these analyses revealed that both transient and stable IE1 expression drastically reduced
193 all types of homology-directed DNA repair (Fig. 3*A-C*, lower panels, and *SI Appendix*, Fig. S3*A-C*). In contrast,
194 IE1 only slightly modulated DNA repair in reporter assays assessing NHEJ (Fig. 3*D*). As the choice between
195 HDR and NHEJ is driven by the cell cycle (45), we confirmed that cell cycle progression was not affected in
196 cells expressing IE1 (*SI Appendix*, Fig. S3*G*). Altogether, these results show that homology-based DNA repair
197 is specifically inhibited in cells expressing HHV-6B IE1.

198

199 **HHV-6B IE1 interacts with NBS1 and inhibits its ability to promote ATM activation**

200 At DSBs, homology-based DNA repair is initiated when lesions are detected by the MRN complex,
201 which leads to ATM auto-activation (Fig. 4*A*) through a still poorly understood mechanism (8, 53, 54). In
202 adenovirus-infected cells, ATM activation is inhibited through the degradation of the MRN complex, which is
203 mediated by the protein E4 (2). In contrast, MRN complex components were stable at steady state upon IE1
204 induction in U2OS clones (Fig. 4*B*). Interestingly, immunofluorescence analyses revealed that IE1 colocalizes
205 with NBS1 in ~75% of IE1-expressing cells (Fig. 4*C-E* and *SI Appendix*, Fig. S4*A-B*). This colocalization was
206 also detected in irradiated cells and *PML* knockout cells (*SI Appendix*, Fig. S4*C-E*), suggesting that the
207 interaction between IE1 and NBS1 is constitutive and independent of PML bodies. We also observed
208 constitutive colocalization between MRE11 and IE1 (Fig. 4*D-E* and *SI Appendix*, Fig. S4*A-B, F*). However, the
209 colocalization of transiently expressed IE1 with MRE11 was greatly reduced upon NBS1 depletion (Fig. 4*F and*
210 *SI Appendix*, Fig. S4*G-H*), supporting a model where IE1 colocalizes with the MRN complex by interacting with
211 NBS1. Importantly, we confirmed that colocalization between IE1 and NBS1 is also observed in HHV-6B-
212 infected MOLT-3 cells (Fig. 4*G-H*).

213 To further characterize the interplay between IE1 and the MRN complex, we took advantage of a cell-
214 based assay that quantifies the ability of a mCherry-LacRnls fusion protein to specifically induce the recruitment
215 of a "prey" to a *LacO* array integrated at a single locus in U2OS 2-6-5 cells (*(i)* No DSBs, Fig. 5A) (55, 56). This
216 system can also be used to study signaling at DSBs by recruiting the ER-mCherry-LacR-FOKI-DD
217 endonuclease to the *LacO* array (*(ii)* Localized DSBs, Fig. 5A). Although ER-mCherry-LacR-FOKI-DD is
218 constitutively expressed in U2OS 2-6-5 cells, the protein is cytoplasmic, and a C-terminal destabilization domain
219 (DD) ensures its continual degradation (55). DSBs can be rapidly induced by adding 4-hydroxytamoxifen (4-
220 OHT) and Shield-1 to the culture medium. 4-OHT induces nuclear relocalization of ER-mCherry-LacR-FOKI-DD
221 *via* its modified estrogen receptor (ER) domain and Shield-1 stabilizes it by inactivating the DD. When the
222 mCherry-LacRnls-IE1 fusion protein was transiently expressed in U2OS 2-6-5 cells, only NBS1 was efficiently
223 recruited to the *LacO* (Fig. 5*B-C* and *SI Appendix*, Fig. S5*A-E*). No DDR signaling proteins were recruited to the
224 *LacO* by the negative control, mCherry-LacRnls. As a positive control, we added 4-OHT and Shield-1 to the
225 medium for 6 h, and readily detected ATM, phospho(p)-ATM (Ser1981), γ-H2AX, RAD50, NBS1, and MRE11.
226 No pATM or γ-H2AX signals were detected at the array upon recruitment of mCherry-LacRnls-IE1, consistent
227 with a constitutive interaction between IE1 and NBS1 that is independent of DSB signaling. Intriguingly, while
228 an mCherry-LacRnls-NBS1 fusion protein is sufficient to induce ATM recruitment and activation, as well as

229 subsequent H2AX phosphorylation at the *LacO* array in NIH-3T3 cells (57), NBS1 recruitment by mCherry-
230 LacRnls-IE1 did not trigger ATM activation (Fig. 5B and *SI Appendix*, Fig. S5*B*). To further validate that IE1
231 inhibits the ability of NBS1 to activate ATM at the *LacO*, we transiently transfected a mCherry-LacRnls-NBS1
232 fusion protein and an untagged or FLAG-tagged IE1 vector in U2OS 2-6-5 cells. As expected, a full length (FL)
233 NBS1 construct (aa 1–754) specifically promoted ATM and H2AX phosphorylation at the *LacO* in approximately
234 75% and 50% of cells, respectively (Fig. 5*D-F* and *SI Appendix*, Fig. S5*F-H*). This function depends on its ability
235 to bind ATM, as an NBS1 ATM binding deficient construct (ΔA) (aa 1–733) produced similar γ-H2AX levels as
236 the negative control (Fig. 5*D* and *SI Appendix*, Fig. S5*F*). Interestingly, NBS1-dependent accumulation of γ-
237 H2AX and pATM was strongly inhibited in cells expressing untagged or FLAG-tagged IE1 (Fig. 5*D-F* and *SI*
238 *Appendix*, Fig. S5*F-H*). These findings suggest that the interaction between IE1 and NBS1 at the array directly
239 prevents ATM activation and subsequent H2AX phosphorylation. In support of this model, we found that IE1
240 accumulates at the *LacO* array upon DSB induction in an NBS1-dependent manner (Fig. 5*G-H*), an observation
241 that can only be made in this system, as no marker of DSB signaling can be used to detect IE1 accumulation at
242 endogenous DSBs. In these conditions, IE1 colocalizes with 60% of mCherry-LacR-FOKI foci and this amount
243 is reduced to 30% in cells treated with a siRNA against NBS1.

244

245 **Two distinct domains of IE1 interact with NBS1 and prevent ATM activation**

246 The functional domains of IE1 are not well characterized aside from its STAT2 binding domain (aa 270–
247 540; Fig. 6*A*) (36). Guided by its secondary structure, we designed a series of IE1 fragments that we fused to
248 mCherry-LacRnls to assess their ability to recruit endogenous NBS1 to the *LacO* array (*SI Appendix*, Fig. S6*A*).
249 The fusion encoding aa 1–540 was the smallest fragment capable of recruiting NBS1 at the *LacO* array as
250 efficiently as FL IE1 (~81% of mCherry-LacRnls-IE1 1–540 colocalized with NBS1; Fig. 6*B-C* and *SI Appendix*,
251 Fig. S6*B*). All attempts to generate smaller fragments of this N-terminal domain of IE1 resulted in unstable
252 proteins in our hands. Interestingly, the 1–540 fragment was also the smallest to efficiently accumulate in PML
253 bodies (*SI Appendix*, Fig. S6*C-D*) suggesting that both functions are related. Consistently, we observed a
254 reduced accumulation of IE1 at PML bodies in cells treated with siNBS1 (*SI Appendix*, Fig. S4*E-F*).
255 To determine if the IE1-NBS1 interaction is sufficient to prevent ATM activation, we transiently
256 transfected expression vectors containing the different fragments of IE1 into U2OS cells (without the *LacO* array)
257 and quantified their ability to inhibit H2AX phosphorylation in irradiated cells. Surprisingly, the IE1 N-terminus
258 alone was unable to prevent the accumulation of γ-H2AX foci (Fig. 6*D-E* and *SI Appendix*, Fig. S6*G*). Instead,
259 we found that this function depends on a fragment of 268 amino acids in the IE1 C-terminus. The 810–1078
260 fragment inhibited H2AX phosphorylation as efficiently as the FL protein (~75% of cells transfected with
261 mCherry-LacRnls-IE1 810–1078 had <10 γ-H2AX foci 1 h post-irradiation with 1 Gy; Fig. 6*D-E* and *SI Appendix*,
262 Fig. S6*G*). Together, these results show that IE1 interacts with NBS1 and blocks ATM activation using two
263 distinct motifs: an N-terminal NBS1-binding domain (NBS1-BD) and a C-terminal domain that independently
264 inhibits the ability of NBS1 to trigger DSB signaling (Fig. 6*A*), which we have named ATM-inhibitory domain
265 (ATMiD).
266 NBS1 encodes a 95-kDa protein with multiple domains, which are required for its recruitment to DSBs
267 and its interactions with the ATM and ATR (58). Briefly, NBS1 contains a forkhead-associated (FHA) domain

268 and two breast cancer C-terminal domains (BRCTs) that are required for optimal phospho-dependent NBS1
269 accumulation at DNA breaks. The C-terminus contains a domain that promotes its interactions with MRE11
270 (MRE11-binding motif, MBM) and ATM (ATM-binding motif, ATM-BM; Fig. 6*F*). Interestingly, NBS1 also
271 contains an intrinsically disordered domain (IDD) that drives a species-specific interaction with the HSV-1 IE
272 protein ICP0 (59). To determine if this domain also promotes the interaction between NBS1 and IE1, we used
273 the same approach used to map the IE1-NBS1 interaction (Fig. 6*A-C*). Different fragments of NBS1 were fused
274 with the mCherry-LacRnls protein and co-expressed with an untagged version of IE1 (Fig. 6*F-H* and *SI*
275 *Appendix*, Fig. S6*H-M*). The mCherry-LacRnls-NBS1 construct lacking the BRCT2 domain (ΔB2, Δaa 201–327)
276 was unable to recruit IE1 to the array, while the construct containing only this domain was sufficient for the
277 interaction (Fig. 6*F-H* and *SI Appendix*, Fig. S6*J, M*). Consistently, immunoprecipitation of FLAG-tagged IE1
278 from U2OS cell lysates revealed an interaction with FL mCherry-LacRnls-NBS1 but not the ΔB2 fusion (Fig. 6*I*).
279 Using the LacR system, we noted that the mCherry-LacRnls-NBS1 fusion lacking the linker region of NBS1 (ΔL,
280 Δ328–638) significantly reduced the interaction between NBS1 and IE1 (*SI Appendix*, Fig. S6*H, J-M*). In contrast
281 with the BRCT2 domain, the linker alone was unable to recruit IE1 to the *LacO* array (*SI Appendix*, Fig. S6*H, J-*
282 *M*).
283 Altogether, our results support a model where the N-terminus of IE1 interacts with the BRCT2 domain
284 of NBS1 and the C-terminus of IE1 blocks ATM activation. In the LacR system, IE1 did not interact with the
285 domain of NBS1 that interacts with ATM (ATM-BM, aa 733–754) (Fig. 6*F-H* and *SI Appendix*, Fig. S6*I, L*) or
286 with ATM itself (Fig. 5*B*). The latter observation suggests that IE1 does not interfere with the NBS1-dependent
287 activation of ATM by directly competing for interactions between them or that the interaction is too weak to be
288 detected in our experimental setting.

289

290 **HHV-6B integration relies on a pathway that safeguards telomere elongation**

291 Depending on the virus, the MRN complex is either required for viral replication or it inhibits it (7). As
292 HHV-6B IE1 interacts with NBS1 and blocks ATM activation, the complex is likely detrimental for its replication.
293 HHV-6B infection has different outcomes depending on the nature of the infected cells (Fig. 7*A*). In permissive
294 cells (*e.g.*, MOLT-3), viral protein expression promotes replication (the lytic state). In contrast, in semi-
295 permissive cells, integration of the viral genome into the host's telomeres is favored, and this process has been
296 proposed to rely on HDR processes in the infected cells (24). To understand the interplay between HHV-6B,
297 DSB signaling, and HDR repair, we investigated the impacts of depleting NBS1 on viral replication and
298 integration. In these experiments, we depleted NBS1 from permissive cells (MOLT-3) and semi-permissive cells
299 (U2OS, HeLa, and GM847) by shRNA (*SI Appendix*, Fig. S6*A-D*). MOLT-3 cells treated with control and NBS1
300 shRNA were infected with HHV-6B and viral DNA was quantified over time by qualitative polymerase chain
301 reaction (qPCR; Fig. 7*B*). Viral DNA replication was 1.67-fold higher in MOLT-3 cells depleted of NBS1 72 h
302 post-infection (note that this is an underestimate, as CellTiter-Glo® assays revealed that the shRNA against
303 NBS1 was toxic in MOLT-3 cells, Fig. 7*C*). Viral integration was assessed in two types of semi-permissive cells:
304 HeLa cells, which lengthen their telomeres *via* hTERT-dependent mechanisms, and U2OS and GM847 cells
305 which rely on ALT, a telomerase-independent mechanism that uses HDR pathways for telomere elongation (60,
306 61). All cell lines were infected with HHV-6B at a multiplicity of infection (MOI) of 1 and passaged for 4 weeks

307 prior to DNA extraction and viral genome quantification by droplet digital (dd)PCR (62). Interestingly, levels of
308 viral integration were approximately 6-fold higher in HeLa cells depleted of NBS1 than in control HeLa cells
309 (Table 1). In contrast, the integration frequency was decreased by at least 2-fold in U2OS and GM847 cell lines
310 depleted of NBS1 vs the control lines. This difference resembles the lower integration level measured in U2OS
311 *PML*$^{-/-}$ cells, a condition previously reported to reduce viral integration (Table 1) (42). NBS1 depletion did not
312 further impact viral integration in these conditions. Lastly, the differences in viral integration levels between the
313 semi-permissive cell lines were not artefactually driven by cell death, as shNBS1 slightly decreased the viability
314 of all cell types used in this study (Fig. 7*C* and *SI Appendix*, Fig. S7E). Altogether, these results are consistent
315 with the need for functional NBS1-dependent HDR repair pathways to promote integration in ALT^{+} cells and
316 support a model where viral integration in semi-permissive cells relies on the molecular mechanisms that drive
317 telomere elongation rather than specific DNA repair mechanisms.

318

319 **Discussion**

320 In this study, we sought to understand how HHV-6B manipulates factors that safeguard genomic
321 instability in infected cells, as well as its impacts on two key events of the viral life cycle: genome replication and
322 chromosomal integration. Using a series of microscopy- and cytometry-based approaches to track the source
323 of DNA breaks in infected cells and in cells expressing the HHV-6B immediate-early protein IE1, we found that
324 IE1 promotes the accumulation of DNA DSBs and inhibits their repair. Further structure-function analyses
325 revealed a molecular mechanism by which HHV-6B IE1 localizes to DSBs in an NBS1-dependent manner and
326 prevents HDR-mediated DNA repair by blocking ATM activation and subsequent DDR signaling. We report that
327 IE1 specifically interacts with NBS1 through an N-terminal NBS1-BD and that ATM activation by NBS1 is
328 strongly inhibited by a newly characterized domain of IE1, the C-terminal ATMiD.

329 ATM activation by the MRN complex requires conformational changes in ATM that expose its substrate-
330 binding site (53). Our findings show that, in contrast with NBS1, IE1 does not interact strongly with ATM in the
331 LacR-based system. Furthermore, the ATMiD domain of IE1 does not interact with NBS1. The exact mechanism
332 by which IE1 inhibits ATM activation thus remains unclear. Based on current literature, IE1 could be interfering
333 with ATM activation by preventing the interaction between the FxF/Y motif of NBS1 and ATM or by directly
334 blocking the substrate-binding site of ATM (53, 63). Alternatively, IE1 may block H2AX phosphorylation through
335 steric hindrance (*e.g.,* though chromatin binding). Viral proteins such as Kaposi's sarcoma-associated
336 herpesvirus LANA and adenovirus protein VII interfere with the activation of chromatin-dependent mechanisms
337 by directly interacting with the nucleosomes (64, 65). Further investigation will be required to elucidate how IE1
338 prevents ATM activation by the MRN complex.

339 The mechanism by which IE1 interacts with NBS1 and inhibits ATM signaling in cells differs from the
340 mechanisms by which other viruses manipulate this pathway (2, 59). The BRCT2 domain of NBS1 contributes
341 to its retention on DSBs (66), which may be reduced when IE1 binds this domain. However, the fact that the IE1
342 N-terminus is insufficient to inhibit ATM signaling suggests otherwise. In this study, we show that IE1 is recruited
343 to DSBs in an NBS1-dependent manner and that ectopic expression of the IE1 ATMiD is sufficient to inhibit
344 DSB signaling. Thus, it is still unclear whether IE1 needs to accumulate at DSBs in an NBS1-dependent manner

345 to inhibit ATM when expressed in infected cells at lower levels, or if NBS1 interaction and ATM inhibition are
346 independent functions of IE1. A model in which IE1 inhibits ATM activation through a bi-partite mechanism is
347 appealing, as it would provide a way for HHV-6B to inhibit ATM signaling at specific loci. This would support a
348 recently proposed concept in which viruses prevent local ATM signaling on the viral genome and restrict viral
349 replication, while avoiding a global inhibition of the DSB signaling cascade in infected cells (67). During the lytic
350 cycle, the accumulation of genomic instability in the host cell genome is not a problem as these cells will die
351 upon the lysis provoked by the virus to release new virus particles. However, more selective inhibition of ATM
352 by IE1 during the latent cycle of HHV-6B or from iciHHV-6B would avoid a detrimental accumulation of genomic
353 alterations in host cells. This model would be consistent with the fact that HHV-6B is not associated with a higher
354 frequency of cancer development, as would be expected if global DSB signaling was inhibited in these cells.
355 Alternatively, expression of IE1 upon the exit of latency may inhibit global DSB signaling, but this phenomenon
356 is restricted to the early stages of the process, thereby minimizing the impact on the host cell's genomic stability.

357 In addition to its role during viral infection, Peddu et al. used RNA-seq approach to show that *IE1 (U90)*
358 is among the most abundantly expressed genes in a variety of tissues from iciHHV-6A/B+ individuals (68).
359 Spontaneous and inducible IE1 protein expression from integrated HHV-6A/B genomes has also been
360 documented (62), raising the possibility that IE1 expression from integrated genomes might contribute to the
361 development of iciHHV-6A/B associated diseases by inducing genomic instability in these cells. At present,
362 conditions associated with iciHHV-6A/B status include increased spontaneous abortion rates (27, 28), pre-
363 eclampsia (29) and angina pectoris (30). Further characterization of the proteins expressed from integrated
364 genomes as well as the diseases associated with these conditions will be required to strengthen our
365 understanding of the consequences associated with viral latency in iciHHV-6A/B subjects. Importantly, the
366 intricate interplay between IE1, the MRN complex, and ATM pathway activation will need to be studied in a
367 spatiotemporal manner to elucidate when and how IE1 manipulates this important pathway during viral infection
368 and integration. Further efforts will also be required to determine if ATM inhibition by IE1 contributes to its ability
369 to block type I interferon signaling in infected cells (36). From a mechanistic point of view, it will be interesting
370 to investigate if the interaction between IE1 and NBS1's BRCT2 domain—a phospho-recognition domain—is
371 regulated by phosphorylation (66, 69–72). Finally, the model presented here assumes that NBS1 and ATM
372 activity must be inhibited to prevent their detrimental effect on viral replication. However, it is impossible to rule
373 out that enhanced viral replication and integration result from the increased level of genomic instability induced
374 in host cells upon viral infection. Further studies will be required to address this question.

375 In germline, hematopoietic, stem, and rapidly renewing cells, telomere elongation relies on hTERT, a
376 polymerase that catalyzes the extension of telomeric DNA repeats using RNA as a template (73). While hTERT
377 is negatively regulated in healthy somatic cells, cancer cells can overcome senescence either through its re-
378 activation or by an alternative homology-directed mechanism called ALT(60). The HHV-6B genome contains
379 conserved telomeric sequences that are required for viral integration (23). In this study, we show that HHV-6B
380 integration is independent of NBS1 in ALT^- cells but dependent on NBS1 in ALT^+ cells. These findings are
381 consistent with previous reports showing that the telomerase complex is required for optimal HHV-6B integration
382 (74) and with the reported role of NBS1 in ALT (75, 76). While PML is not required for the IE1-NBS1 interaction
383 or the ability of IE1 to inhibit H2AX phosphorylation (this study), NBS1 is required for the assembly of functional

384 ALT-associated PML bodies (77). These concomitant roles are in line with the absence of phenotypes
385 associated with NBS1 depletion in integration assays performed on *PML*$^{-/-}$ ALT^{+} U2OS cells. Intriguingly, we
386 previously reported that *PML* knockout also reduces integration in ALT^{-} HeLa cells, reinforcing the hypothesis
387 that PML plays an ALT-independent role in this process (42). Further studies will be required to elucidate this
388 function.

389 Consistent with previous findings showing that HHV-6B integration is not altered upon inhibition of
390 RAD51 (78, 79), we found that IE1 inhibits HDR processes, and that integration is independent of NBS1 in ALT-
391 cell lines. Together, these observations argue against models where integration mechanisms rely on RAD51-
392 dependent BIR or SSA (24). However, it is important to note that all homology-directed reporter assays used in
393 this study rely on extensive DNA end resection following nuclease-induced breakage, a process that is
394 dependent on NBS1 (80). Thereby, integration models where SSA or RAD51-independent BIR trigger
395 integration following extensive accumulation of ssDNA generated at stalled replication forks remain plausible.
396 One attractive model is that HHV-6B integration occurs during mitotic DNA synthesis (MiDAS), a RAD52-
397 dependent BIR mechanism that is initiated by replication fork stalls that remain unresolved at the start of
398 mitosis—a problem often observed at hard-to-replicate loci, including the telomeres (13, 27, 81). Alternatively,
399 upon cell entry but before viral genome circularization (and before IE1 is expressed), the viral genome may be
400 perceived as broken DNA. Under such circumstances, the MRN complex would be recruited to the ends of the
401 viral genome and initiate 3′→ 5′ resections. The ssDNA ends of eroded telomeres (no longer efficiently protected
402 by the shelterin complex) could anneal to the near-terminal telomeric sequence at the right end of the genome
403 in a process analogous to an ALT mechanism described in yeast (reviewed in (13)). Once the entire viral
404 genome is copied, the telomeric repeats at the left end of the genome would serve as a template for the hTERT
405 and ALT mechanisms to regenerate a telomere of appropriate length (82).

406 In conclusion, we provide a detailed characterization of the HHV-6B IE1 protein as an efficient inhibitor
407 of DSB signaling and DDR that contributes to the favorable establishment of a productive infection. Despite
408 being a relatively abundant protein expressed very early upon entry, the functions of IE1 remain poorly defined.
409 IE1 shares very little sequence homology with proteins from other herpesviruses (except HHV-6A and HHV-7)
410 meaning that deductions based on primary sequence analysis are very limited. Our work adds to the growing
411 knowledge surrounding HHV-6B integration processes and the potential importance of IE1 during infection.

412

413 **Materials and Methods**

414 **RNA interference**

415 A SMARTPool siRNA targeting RAD51, single siRNA duplexes targeting NBS1, and a non-targeting single
416 siRNA duplex were purchased from Dharmacon (Horizon). Single siRNA duplexes targeting RAD52 were a kind
417 gift from Jean-Yves Masson (Université Laval, Québec, Canada). siRNAs were forward-transfected 24 h prior
418 to cell processing using RNAimax (Invitrogen) according to the manufacturer's protocol. Plasmids carrying an
419 NBS1 shRNA (Open Biosystems) or a control shRNA (Sigma) in the pLKO background backbone were a kind
420 gift from Cary A. Moody (6). Lentiviruses were produced as previously described (6). Briefly, plasmids
421 expressing shRNAs with vesicular stomatitis virus G (pMD2.g) and lentiviral packaging (pPAX) plasmids were

422 co-transfected into HEK293T cells using polyethyleneimine. Lentivirus-containing supernatants were harvested
423 48–72 h post-transfection, and U2OS, MOLT-3, HeLa, and GM847 cells were transduced in the presence of 8
424 µg/mL Polybrene (Sigma). For all relevant experiments, RAD51, RAD52, and NBS1 depletion was confirmed
425 by immunoblotting or qPCR analyses.
426
427 **Cell cultures and transfections**
428 Cell lines were maintained at 37°C and 5% CO_2. All culture media were supplemented with 10% fetal bovine
429 serum. MOLT-3 cells (American Type Culture Collection (ATCC)) were cultured in Roswell Park Memorial
430 Institute-1640 (RPMI) medium (Corning Cellgro), 8.85 mM HEPES, and 5 µg/mL plasmocin (Invivogen). GM847
431 and HeLa cell lines were obtained from ATCC and cultured in Dulbecco's modified Eagle's medium (DMEM;
432 Corning Cellgro), NEM (Corning Cellgro), 8.85 mM HEPES, and 5 µg/mL plasmocin. U2OS (ATCC), U2OS
433 *PML*$^{-/-}$ (42), U2OS 2-6-5 (a kind gift from Roger Greenberg, University of Pennsylvania, Philadelphia) (55), U2OS
434 DR-GFP, SA-GFP (a kind gift from Jeremy Stark, City of Hope National Medical Center, California) (48, 52),
435 and cell lines were cultured in McCoy's medium (Life Technologies).
436
437 **Viral infection and integration assays**
438 Viral infection was done as previously described (42) using HHV-6B (strain Z29) at an MOI of 1 (or not (Mock
439 samples)). At the indicated time points, cells were harvested and processed for DNA extraction using a QIAamp
440 DNA Blood Mini Kit (Qiagen) and analyzed by qPCR. Integration assays were performed as described
441 previously (62). Briefly, cells were infected with HHV-6B (MOI of 1) for 24 h and passaged for 4 weeks prior to
442 DNA extraction with the QIAamp DNA Blood Mini Kit for ddPCR.
443
444 **PCR analyses**
445 qPCR was performed as previously described (83). DNA was quantified using primers and probes against *U67-*
446 *68* (HHV-6B) and ribonuclease P/MRP subunit p30 (*RPP30*; as a host reference gene). Data were normalized
447 against the corresponding genome copies of *RPP30*. ddPCR was used to quantify integration frequency as
448 previously described (62). Briefly, HHV-6B chromosomal integration frequencies were estimated assuming a
449 single integrated HHV-6/cell and calculated with the following formula: (number of HHV-6 copies)/(number of
450 *RPP30* copies/2 copies per cell) × 100, as previously described (62). This assay has been extensively validated
451 and provides comparable data to single cell cloning and quantification.
452
453 **Immunofluorescence microscopy**
454 Immunofluorescence were done essentially as previously described for MOLT-3 (42) and U2OS (56) cells.
455 Briefly, cells were either fixed with 2% paraformaldehyde (PFA) or 100% MeOH prior to permeabilization and
456 incubation with primary antibody diluted in blocking buffer. DNA was counterstained with DAPI and the
457 coverslips were mounted onto glass slides with Prolong Diamond Mounting Agent (Invitrogen). Further
458 experimental details are provided as the Supplementary information.
459
460 **FISH**

461 Fixed cells were processed as described for immunofluorescence staining and then fixed for 2 min at room
462 temperature with 1% PFA/PBS. Coverslips were washed twice with PBS for 5 min and dehydrated for 5 min in
463 successive ethanol baths (70%, 95%, 100%). Once dried, coverslips were placed upside down on a drop of
464 hybridizing solution (70% formamide, 0.5% blocking reagent (Sigma, Cat:11096176001), 10 mM Tris-HCl pH
465 7.2, 1/1000 Cy5-TelC PNA probe (F1003, PNABio)). Samples were denatured for 10 min at 80°C on a heated
466 block, then incubated overnight at 4°C in the dark. After hybridization, coverslips were washed twice for 15 min
467 in washing solution (70% formamide; 10 mM Tris-HCl pH 7.2) and then washed three times for 5 min with PBS.
468 Coverslips were air-dried, counterstained with DAPI, washed with PBS, and mounted onto glass slides with
469 Prolong Gold Mounting Agent.
470
471 **Metaphase spread analysis**
472 U2OS SA-GFP HHV-6B IE1 cells were arrested in mitosis using 1 μM nocodazole for 3 h at 37°C and 5% CO_2.
473 Cells were then resuspended and incubated in pre-warmed hypotonic solution (KCl 75 mM, 15% fetal bovine
474 serum) at 37°C for 15 min to induce swelling and fixed in a 75% ethanol 25% acetic acid solution overnight at
475 4°C. Droplets of cells were spread onto glass slides pre-cooled to -20°C and dried overnight in the dark at room
476 temperature. Slides were then mounted with Vectashield Antifade Mounting Medium containing DAPI
477 (VECTH20002, MJS BioLynx Inc.). Images were acquired using a Zeiss LSM700 laser-scanning microscope
478 equipped with a 40× water lens. Quantification was performed on three biological replicates and 10 spreads
479 were quantified per experiment.
480
481 **Immunoprecipitation**
482 U2OS cells (1×10^7) were transfected with NBS1- or non-targeting single siRNA duplexes for 24 h, then co-
483 transfected with the indicated mCherry-LacR and 3×FLAG expression vectors. After 24 h, cells were lysed in
484 NETN lysis buffer (50 mM Tris pH 8.0, 150 mM NaCl, 1mM EDTA, 0.5% NP-40) complemented with 1×
485 complete, EDTA-free Protease Inhibitor Cocktail (Roche), 20 mM N-ethylmethylamine, 1 mM NaF, and 0.2 mM
486 Na_3VO_4. Cleared cell lysates were immunoprecipitated using 1 μg FLAG-M2 antibody coupled to 40 μL of
487 packed protein G Sepharose beads (Cat GE17-0618-01, Sigma) for 3 h at 4°C. Beads were washed four times
488 with NETN buffer and eluted in 2× Laemmli buffer for immunoblotting.
489
490 **Reporter-based DNA repair assays**
491 DR-GFP, NHEJ-GFP, SA-GFP, and BIR-GFP cell lines were plated at 125,000 cells/well in 6-well plates. After
492 24 h, cells were co-transfected with 900 ng of the I-SceI plasmid (pCBASceI, Addgene #26477) and 900 ng of
493 pcDNA4/TO-HHV-6B IE1 (+I-SceI, +IE1) or 900 ng of the pcDNA4/TO/Myc-His vector as a negative control (+I-
494 SceI, -IE1). The pcDNA4/TO/myc-His vector alone was transfected for conditions without IE1 and I-SceI (-I-
495 SceI/-IE1). A plasmid expressing iRFP (200 ng) was also transfected into all conditions to control for transfection
496 efficiency. After 48 h, cells were harvested and washed with PBS, and an Accuri C6 flow cytometer (BD
497 Biosciences) was used to quantify the GFP^+ cells in the $iRFP^+$ population. Data were analyzed using FlowJo.
498 The NHEJ-GFP (EJ7) assay was performed essentially as described above, but cells were co-transfected with
499 600 ng of each Cas9/sgRNA-expressing vector p330X-sgRNA7a, and p330X-sgRNA7b along with 600 ng of

pcDNA4/TO-HHV-6B IE1 or pcDNA4/TO/myc-His (52) and processed for flow cytometry analysis 72 h post-transfection.

Statistical analysis

Quantifications were performed on three biological replicates. Unless otherwise stated, one-way analysis of variance and Dunnett's multiple comparisons test were used to assess statistical significance.

Acknowledgements

We are grateful to Matthew D. Weitzman, Alexandre Orthwein, Cary A. Moody, and members of the Fradet-Turcotte and Flamand laboratories for critical reading of the manuscript; High-Fidelity Science Communications for manuscript editing, and Daniel Durocher, Jean-Yves Masson, Graham Dellaire, Roger Greenberg, and Jeremy Stark for essential reagents. E.B, and V.C. received postdoctoral and doctoral fellowships, respectively, from the Fonds de Recherche du Québec - Santé. V.T. received a master's fellowship from the Fonds de recherche Nature et technologies. This work was supported by three Canadian Institutes of Health Research Grants (PJT_152948 to A.F.-T.; MOP_123214 and PJT_156118 to L.F.). A.F.-T. is a Tier 2 Canada Research Chair in Molecular Virology and Genomic Instability and is supported by the Foundation J.-Louis Lévesque. We thank the Bioimaging platform of the Infectious Disease Research Centre, which is funded by an equipment and infrastructure grant from the Canadian Foundation for Innovation.

References

1. J. L. Justice, I. M. Cristea, Nuclear antiviral innate responses at the intersection of DNA sensing and DNA repair. *Trends Microbiol* **TBD** (2022).
2. T. H. Stracker, C. T. Carson, M. D. Weilzman, Adenovirus oncoproteins inactivate the Mre11-Rad50-NBs1 DNA repair complex. *Nature* **418** (2002).
3. S. S. Lakdawala, *et al.*, Differential Requirements of the C Terminus of Nbs1 in Suppressing Adenovirus DNA Replication and Promoting Concatemer Formation. *J Virol* **82** (2008).
4. C. E. Lilley, C. T. Carson, A. R. Muotri, F. H. Gage, M. D. Weitzman, DNA repair proteins affect the lifecycle of herpes simplex virus 1. *Proc Natl Acad Sci U S A* **102** (2005).
5. C. A. Moody, L. A. Laimins, Human papillomaviruses activate the ATM DNA damage pathway for viral genome amplification upon differentiation. *PLoS Pathog* **5** (2009).
6. D. C. Anacker, D. Gautam, K. A. Gillespie, W. H. Chappell, C. A. Moody, Productive Replication of Human Papillomavirus 31 Requires DNA Repair Factor Nbs1. *J Virol* **88**, 8528–8544 (2014).
7. M. D. Weitzman, A. Fradet-Turcotte, Virus DNA replication and the host DNA damage response. *Annu Rev Virol* **5** (2018).
8. A. Syed, J. A. Tainer, The MRE11-RAD50-NBS1 Complex Conducts the Orchestration of Damage Signaling and Outcomes to Stress in DNA Replication and Repair. *Annu Rev Biochem* **87** (2018).

536 9. A. Fradet-Turcotte, *et al.*, 53BP1 is a reader of the DNA-damage-induced H2A Lys 15 ubiquitin mark.
537 *Nature* **499** (2013).

538 10. F. Mattiroli, L. Penengo, Histone Ubiquitination: An Integrative Signaling Platform in Genome
539 Stability. *Trends in Genetics* (2021) https:/doi.org/10.1016/j.tig.2020.12.005.

540 11. L. Krenning, J. van den Berg, R. H. Medema, Life or Death after a Break: What Determines the Choice?
541 *Mol Cell* **76** (2019).

542 12. A. Maréchal, L. Zou, DNA damage sensing by the ATM and ATR kinases. *Cold Spring Harb Perspect Biol*
543 **5** (2013).

544 13. Z. W. Kockler, B. Osia, R. Lee, K. Musmaker, A. Malkova, Repair of DNA Breaks by Break-Induced
545 Replication. *Annu Rev Biochem* **90** (2021).

546 14. R. Bhargava, D. O. Onyango, J. M. Stark, Regulation of Single Strand Annealing and its role in genome
547 maintenance Chromosomal break repair by the Single Strand Annealing (SSA) pathway. *Trends Genet*
548 **32**, 566–575 (2016).

549 15. J. Kramara, B. Osia, A. Malkova, Break-Induced Replication: The Where, The Why, and The How.
550 *Trends in Genetics* **34**, 518–531 (2018).

551 16. K. Yamanishi, *et al.*, Identification of Human Herpesvirus-6 As a Causal Agent for Exanthem Subitum.
552 *The Lancet* **331**, 1065–1067 (1988).

553 17. D. M. Zerr, *et al.*, A Population-Based Study of Primary Human Herpesvirus 6 Infection. *New England*
554 *Journal of Medicine* **352**, 768–776 (2005).

555 18. C. B. Hall, *et al.*, Congenital infections with human herpesvirus 6 (HHV6) and human herpesvirus 7
556 (HHV7). *Journal of Pediatrics* **145**, 472–477 (2004).

557 19. V. Collin, L. Flamand, HHV-6A/B integration and the pathogenesis associated with the reactivation of
558 chromosomally integrated HHV-6A/B. *Viruses* **9** (2017).

559 20. S. N. Pantry, P. G. Medveczky, Latency, integration, and reactivation of human herpesvirus-6. *Viruses*
560 **9** (2017).

561 21. J. H. Arbuckle, *et al.*, Mapping the telomere integrated genome of human herpesvirus 6A and 6B.
562 *Virology* **442**, 3–11 (2013).

563 22. J. H. Arbuckle, *et al.*, The latent human herpesvirus-6A genome specifically integrates in telomeres of
564 human chromosomes in vivo and in vitro. *Proc Natl Acad Sci U S A* **107**, 5563–5568 (2010).

565 23. N. Wallaschek, *et al.*, The Telomeric Repeats of Human Herpesvirus 6A (HHV-6A) Are Required for
566 Efficient Virus Integration. *PLoS Pathog* **12**, 1–15 (2016).

567 24. G. Aimola, G. Beythien, A. Aswad, B. B. Kaufer, Current understanding of human herpesvirus 6 (HHV-
568 6) chromosomal integration. *Antiviral Res* **176** (2020).

569 25. K. Tanaka-Taya, *et al.*, Human herpesvirus 6 (HHV-6) is transmitted from parent to child in an
570 integrated form and characterization of cases with chromosomally integrated HHV-6 DNA. *Journal of*
571 *Medical VirologyThe prevalence of chromosomally integrated human herpesvirus 6 genomes in the*
572 *blood of UK blood donors.* **73**, 465–473 (2004).

573 26. M. Daibata, T. Taguchi, Y. Nemoto, H. Taguchi, I. Miyoshi, Inheritance of chromosomally integrated
574 human herpesvirus 6 DNA. *Blood* **94**, 1545–1549 (1999).

575 27. S. Minocherhomji, *et al.*, Replication stress activates DNA repair synthesis in mitosis. *Nature* **528**
576 (2015).

577 28. H. Miura, *et al.*, Inherited Chromosomally Integrated Human Herpesvirus 6 Is a Risk Factor for
578 Spontaneous Abortion. *J Infect Dis* **223** (2021).

579 29. F. Gaccioli, *et al.*, Fetal inheritance of chromosomally integrated human herpesvirus 6 predisposes the
580 mother to pre-eclampsia. *Nat Microbiol* **5** (2020).

581 30. A. Gravel, *et al.*, Inherited chromosomally integrated human herpesvirus 6 as a predisposing risk
582 factor for the development of angina pectoris. *Proc Natl Acad Sci U S A* **112** (2015).

583 31. P. E. Pellett, Chromosomally integrated human herpesvirus 6: questions and answers. *Rev Med Virol*
584 **22**, 144–55 (2012).

585 32. L. Flamand, "Chromosomal integration by human herpesviruses 6A and 6B" in *Advances in*
586 *Experimental Medicine and Biology*, (2018).

587 33. A. Gravel, *et al.*, Mapping the Human Herpesvirus 6B transcriptome. *J Virol* (2021)
588 https:/doi.org/10.1128/JVI.01335-20.

589 34. U. Schiewe, F. Neipel, D. Schreiner, B. Fleckenstein, Structure and transcription of an immediate-early
590 region in the human herpesvirus 6 genome. *J Virol* **68**, 2978–2985 (1994).

591 35. J. Jaworska, A. Gravel, K. Fink, N. Grandvaux, L. Flamand, Inhibition of Transcription of the Beta
592 Interferon Gene by the Human Herpesvirus 6 Immediate-Early 1 Protein. *J Virol* **81**, 5737–5748
593 (2007).

594 36. J. Jaworska, A. Gravel, L. Flamand, Divergent susceptibilities of human herpesvirus 6 variants to type I
595 interferons. *Proc Natl Acad Sci U S A* **107**, 8369–8374 (2010).

596 37. R. Bernardi, P. P. Pandolfi, Structure, dynamics and functions of promyelocytic leukaemia nuclear
597 bodies. *Nat Rev Mol Cell Biol* **8**, 1006–1016 (2007).

598 38. P. L. Yeung, *et al.*, Promyelocytic leukemia nuclear bodies support a late step in DNA double-strand
599 break repair by homologous recombination. *J Cell Biochem* **113**, 1787–1799 (2012).

600 39. K. M. Attwood, *et al.*, PML isoform expression and DNA break location relative to PML nuclear bodies
601 impacts the efficiency of homologous recombination. *Biochemistry and Cell Biology*, 1–42 (2019).

602 40. G. Dellaire, *et al.*, Promyelocytic leukemia nuclear bodies behave as DNA damage sensors whose
603 response to DNA double-strand breaks is regulated by NBS1 and the kinases ATM, Chk2, and ATR.
604 *Journal of Cell Biology* **175**, 55–66 (2006).

605 41. M. Vancurova, *et al.*, PML nuclear bodies are recruited to persistent DNA damage lesions in an
606 RNF168-53BP1 dependent manner and contribute to DNA repair. *DNA Repair (Amst)* **78** (2019).

607 42. V. Collin, A. Gravel, B. B. Kaufer, L. Flamand, The promyelocytic leukemia protein facilitates human
608 herpesvirus 6B chromosomal integration, immediate-early 1 protein multiSUMOylation and its
609 localization at telomeres. *PLoS Pathog* **16** (2020).

610 43. A. P. R. Cassel, R. B. Barcellos, C. M. D. da Silva, S. E. de Matos Almeida, M. L. R. Rossetti, Association
611 between human papillomavirus (HPV) DNA and micronuclei in normal cervical cytology. *Genet Mol*
612 *Biol* **37**, 360–363 (2014).

613 44. E. M. Hatch, A. H. Fischer, T. J. Deerinck, M. W. Hetzer, Catastrophic Nuclear Envelope Collapse in
614 Cancer Cell Micronuclei. *Cell* **154** (2013).

615 45. N. Hustedt, D. Durocher, The control of DNA repair by the cell cycle. *Nat Cell Biol* **19**, 1–9 (2017).

616 46. B. van de Kooij, H. van Attikum, Genomic Reporter Constructs to Monitor Pathway-Specific Repair of
617 DNA Double-Strand Breaks. *Front Genet* **12** (2022).

618 47. J. Pinder, J. Salsman, G. Dellaire, Nuclear domain "knock-in" screen for the evaluation and
619 identification of small molecule enhancers of CRISPR-based genome editing. *Nucleic Acids Res* **43**
620 (2015).

621 48. J. M. Stark, A. J. Pierce, J. Oh, A. Pastink, M. Jasin, Genetic Steps of Mammalian Homologous Repair
622 with Distinct Mutagenic Consequences. *Mol Cell Biol* **24**, 9305–9316 (2004).

623 49. R. A. C. M. Boonen, *et al.*, Functional analysis of genetic variants in the high-risk breast cancer
624 susceptibility gene PALB2. *Nat Commun* **10** (2019).

625 50. L. Costantino, *et al.*, Break-induced replication repair of damaged forks induces genomic duplications
626 in human cells. *Science (1979)* **343**, 88–91 (2014).

627 51. K. Jacquet, *et al.*, The TIP60 Complex Regulates Bivalent Chromatin Recognition by 53BP1 through
628 Direct H4K20me Binding and H2AK15 Acetylation. *Mol Cell* **62**, 409–421 (2016).

629 52. R. Bhargava, *et al.*, C-NHEJ without indels is robust and requires synergistic function of distinct XLF
630 domains. *Nat Commun* **9** (2018).

631 53. C. Warren, N. P. Pavletich, Structure of the human ATM kinase and mechanism of Nbs1 binding. *Elife*
632 **11** (2022).

633 54. C. B. Schiller, *et al.*, Structure of Mre11-Nbs1 complex yields insights into ataxia-telangiectasia- like
634 disease mutations and DNA damage signaling. *Nat Struct Mol Biol* **19** (2012).

635 55. J. Tang, *et al.*, Acetylation limits 53BP1 association with damaged chromatin to promote homologous
636 recombination. *Nat Struct Mol Biol* **20**, 317–325 (2013).

637 56. J. Sitz, *et al.*, Human papillomavirus E7 oncoprotein targets RNF168 to hijack the host DNA damage
638 response. *Proc Natl Acad Sci U S A* **116**, 19552–19562 (2019).

639 57. E. Soutoglou, T. Misteli, Activation of the cellular DNA damage response in the absence of DNA
640 lesions. *Science (1979)* **320** (2008).

641 58. L. Bian, Y. Meng, M. Zhang, D. Li, MRE11-RAD50-NBS1 complex alterations and DNA damage
642 response: Implications for cancer treatment. *Mol Cancer* **18** (2019).

643 59. D. I. Lou, *et al.*, An Intrinsically Disordered Region of the DNA Repair Protein Nbs1 Is a Species-Specific
644 Barrier to Herpes Simplex Virus 1 in Primates. *Cell Host Microbe* **20** (2016).

645 60. A. J. Cesare, R. R. Reddel, Alternative lengthening of telomeres: Models, mechanisms and
646 implications. *Nat Rev Genet* **11** (2010).

647 61. R. L. Dilley, *et al.*, Break-induced telomere synthesis underlies alternative telomere maintenance.
648 *Nature* **539** (2016).

649 62. A. Gravel, *et al.*, Cell Culture Systems To Study Human Herpesvirus 6A/B Chromosomal Integration. *J*
650 *Virol* **91**, e00437-17 (2017).

651 63. Z. You, C. Chahwan, J. Bailis, T. Hunter, P. Russell, ATM Activation and Its Recruitment to Damaged
652 DNA Require Binding to the C Terminus of Nbs1. *Mol Cell Biol* **25** (2005).

653 64. A. J. Barbera, *et al.*, The nucleosomal surface as a docking station for Kaposi's sarcoma herpesvirus
654 LANA. *Science (1979)* **311** (2006).

655 65. D. C. Avgousti, *et al.*, A core viral protein binds host nucleosomes to sequester immune danger
656 signals. *Nature* **535** (2016).

657 66. C. Lukas, *et al.*, Mdc1 couples DNA double-strand break recognition by Nbs1 with its H2AX-dependent
658 chromatin retention. *EMBO Journal* **23** (2004).

659 67. G. A. Shah, C. C. O'Shea, Viral and Cellular Genomes Activate Distinct DNA Damage Responses. *Cell*
660 **162** (2015).

661 68. V. Peddu, *et al.*, Inherited Chromosomally Integrated Human Herpesvirus 6 Demonstrates Tissue-
662 Specific RNA Expression In Vivo That Correlates with an Increased Antibody Immune Response . *J Virol*
663 **94** (2019).

664 69. F. J. Hari, C. Spycher, S. Jungmichel, L. Pavic, M. Stucki, A divalent FHA/BRCT-binding mechanism
665 couples the MRE11-RAD50-NBS1 complex to damaged chromatin. *EMBO Rep* **11** (2010).

666 70. J. R. Chapman, S. P. Jackson, Phospho-dependent interactions between NBS1 and MDC1 mediate
667 chromatin retention of the MRN complex at sites of DNA damage. *EMBO Rep* **9** (2008).

668 71. K. Kim, T. W. Kirby, L. Perera, R. E. London, Phosphopeptide interactions of the Nbs1 N-terminal FHA-
669 BRCT1/2 domains. *Sci Rep* **11** (2021).

670 72. C. Xu, *et al.*, Structure of a Second BRCT Domain Identified in the Nijmegen Breakage Syndrome
671 Protein Nbs1 and its Function in an MDC1-Dependent Localization of Nbs1 to DNA Damage Sites. *J*
672 *Mol Biol* **381** (2008).

673 73. R. A. Wu, H. E. Upton, J. M. Vogan, K. Collins, Telomerase mechanism of telomere synthesis. *Annu Rev*
674 *Biochem* **86** (2017).

675 74. S. Gilbert-Girard, *et al.*, Stabilization of telomere G-quadruplexes interferes with human herpesvirus
676 6A chromosomal integration. *J Virol*, JVI.00402-17 (2017).

677 75. Z. H. Zhong, *et al.*, Disruption of telomere maintenance by depletion of the MRE11/RAD50/NBS1
678 complex in cells that use alternative lengthening of telomeres. *Journal of Biological Chemistry* **282**
679 (2007).

680 76. W.-Q. Jiang, *et al.*, Suppression of Alternative Lengthening of Telomeres by Sp100-Mediated
681 Sequestration of the MRE11/RAD50/NBS1 Complex. *Mol Cell Biol* **25** (2005).

682 77. G. Wu, X. Jiang, W. H. Lee, P. L. Chen, Assembly of functional ALT-associated promyelocytic leukemia
683 bodies requires nijmegen breakage syndrome 1. *Cancer Res* **63** (2003).

684 78. D. J. Wight, *et al.*, Viral proteins U41 and U70 of human herpesvirus 6A are dispensable for telomere
685 integration. *Viruses* **10** (2018).

686 79. N. Wallaschek, A. Gravel, L. Flamand, B. B. Kaufer, The putative U94 integrase is dispensable for
687 human herpesvirus 6 (HHV-6) chromosomal integration. *Journal of General Virology* **97** (2016).

688 80. S. Sakamoto, *et al.*, Homologous recombination repair is regulated by domains at the N- and C-
689 terminus of NBS1 and is dissociated with ATM functions. *Oncogene* **26** (2007).

690 81. R. Bhowmick, S. Minocherhomji, I. D. Hickson, RAD52 Facilitates Mitotic DNA Synthesis Following
691 Replication Stress. *Mol Cell* **64** (2016).

692 82. Y. Huang, *et al.*, Human telomeres that carry an integrated copy of human herpesvirus 6 are often
693 short and unstable, facilitating release of the viral genome from the chromosome. *Nucleic Acids Res*
694 **42** (2014).

695 83. A. Gravel, J. Gosselin, L. Flamand, Human herpesvirus 6 immediate-early 1 protein is a sumoylated
696 nuclear phosphoprotein colocalizing with promyelocytic leukemia protein-associated nuclear bodies.
697 *Journal of Biological Chemistry* **277**, 19679–19687 (2002).

698

699 **Figure Legends**

700 **Fig. 1.** HHV-6B infection and IE1 expression lead to micronuclei formation *(A)* Left panel: Representative images
701 of Mock and HHV-6B-infected MOLT-3 cells fixed 24 h post-infection and counterstained with DAPI. Micronuclei
702 are indicated by white arrows. The quantification of the micronuclei (right panel) shows the mean (n = 2, >100
703 micronuclei/condition). *(B)* Left panel: representative images of U2OS cell lines and clones stably expressing
704 Dox-inducible HHV-6B IE1 (C10 and C102). IE1 expression was induced with 1 µg/mL Dox for 48 h prior to IE1
705 immunofluorescence. Micronuclei are indicated by white arrows. The parental cell line (Par.) was used as a
706 negative control. The micronuclei (right panel) quantification shows the mean ± standard deviation (SD; n = 3).
707 *(C)* Schematic of micronuclei formation *via* DNA double-strand breaks (DSBs) (i), lagging chromosomes (ii),
708 and anaphase bridges (ABs) (iii). *(D-E)* Quantification of micronuclei containing centromeres (D) and telomeres
709 (E). Cells were treated as in B and centromeres and telomeres were detected by immunofluorescence and
710 FISH, respectively. Data represent the mean ± SD (n = 3) (D) and the mean (n = 2, > 100 micronuclei/condition)
711 (E). *(F)* A representative metaphase spread from an IE1-expressing cell. Cells were treated with 1 µg/mL Dox
712 for 48 h, then metaphase spreads were prepared, fixed, and counterstained with DAPI. *(G)* Quantification of
713 chromosomal aberrations per metaphase. Data represent the mean ± SD (n = 31). **p < 0.01, ***p < 0.001,
714 ****p < 0.0001. Scale bars = 5 µm.

715

716 **Fig. 2.** H2AX phosphorylation (γ-H2AX) is inhibited in HHV-6B-infected and IE1-expressing cells *(A)*
717 Representative γ-H2AX immunostaining in HHV-6B-infected MOLT-3 cells irradiated with 4 Gy and
718 immunostained for IE1 and γ-H2AX 1 h later. Mock-infected cells were used as a negative control. *(B)*
719 Quantification of irradiated MOLT-3-infected and Mock cells with > 10 γ-H2AX foci. Data represent the mean ±
720 SD (n = 3). Statistical significance was assessed using unpaired *t*-test. *(C)* Representative γ-H2AX
721 immunostaining in irradiated U2OS parental (Par.) and IE1-expressing cells (Clone C10). IE1 expression was

722 induced as in Fig. 1B. Cells were irradiated with 1 Gy and immunostained for IE1 and γ-H2AX 1 h later. *(D)*
723 Quantification of irradiated U2OS Par. and IE1-expressing cells with > 10 γ-H2AX foci. Data are presented as
724 the mean ± SD (*n* = 3). *(E)* Quantification of cells with > 10 γ-H2AX foci in irradiated (1 Gy) U2OS *PML*$^{+/+}$ and $^{-}$
725 $^{/-}$ cells that transiently express untagged IE1. An empty vector (EV) was used as a negative control. Data
726 represent the mean ± SD (*n* = 3). ****$p < 0.0001$. Scale bars = 5 μm.
727

728 **Fig. 3.** HHV-6B IE1 inhibits HDR-mediated repair *(A-D)* DNA repair reporter assays for (A) homologous
729 recombination (DR-GFP), (B) single-strand annealing (SA-GFP), (C) break-induced replication (BIR-GFP), and
730 (D) non-homologous end-joining (NHEJ-GFP (EJ7)). For each assay, a schematic is presented in the top panel
731 and the flow cytometry-based quantification of GFP^{+} cells is presented in the bottom panel. In each replicate,
732 GFP^{+} cells were normalized to the GFP^{+} cells in the positive control (I-SceI^{+} or Cas9^{+}, set to 1.0). Data represent
733 the mean ± SD (*n* = 3). ****p < 0.0001.
734

735 **Fig. 4.** HHV-6B IE1 colocalizes with NBS1 *(A)* Signaling events triggered by DNA DSBs. *(B)* Whole cell extracts
736 (WCEs) from U2OS cells (Par.) and IE1-expressing U2OS stable cell lines treated with or without 1 μg/mL Dox
737 were immunoblotted for RAD50, NBS1, and MRE11. GAPDH was used as a loading control. *(C, E)*
738 Representative images of the colocalization between IE1 and NBS1 (C) and MRE11 (E). IE1-expressing cells
739 were treated as described in Fig. 1B and immunostained for IE1, NBS1, or MRE11. As a positive control,
740 irradiated U2OS cells (+IR) were fixed 15 min post-irradiation (1 Gy) and immunostained as indicated (*SI*
741 *Appendix*, Fig. S4*A*; scale bars, 5 μm). The parental cell line (Par.) was used as a negative control. *(D)*
742 Percentages of IE1 foci that colocalized with NBS1 (C) and MRE11 (E). Data represent the mean ± SD of three
743 independent experiments. *(F)* Percentage of IE1 foci that colocalized with MRE11 in stable U2OS control cells
744 (shCTRL) or those depleted of NBS1 (shNBS1). Data represent the mean ± SD (*n* = 2, at least 40
745 nuclei/condition). Statistical significance was assessed using unpaired *t*-test. ****$p < 0.0001$. Scale bars = 5 μm.
746

747 **Fig. 5.** HHV-6B IE1 interacts with NBS1, inhibits ATM activation, and is recruited to DSBs *(A)* The integrated
748 *LacO* array-based assay used to study protein colocalization at a specific locus without DSBs (*i*) or DNA repair
749 protein recruitment at localized DSBs (*ii*). *LacO* array repeats, mCherry-LacRnls-fusion proteins, and preys are
750 shown in grey, red/orange, and green, respectively. *(B)* Quantification of the indicated DSB-signaling proteins
751 at localized DSBs induced by ER-mCherry-LacRnls-FOKI-DD (FOKI) or at either a mCherry-LacRnls (--,
752 negative control) or mCherry-LacRnls HHV-6B IE1 protein foci in U2OS 2-6-5 cells. Transfected cells were
753 treated with 4-OHT and Shield-1 for 6 h then immunostained for ATM, pATM (S1981), γ-H2AX, RAD50, NBS1,
754 and MRE11 (Representative images, *SI Appendix,* Fig. S5*A-E)*. For each condition, statistical significance was
755 analyzed against the control protein (mCherry-LacRnls). Data represent the mean ± SD (*n* = 3). *(C)*
756 Representative images of NBS1 recruitment at DSBs (top panel) and its colocalization with IE1 in the absence
757 of DSBs (bottom panel). *(D-E)* U2OS 2-6-5 cells were treated as described in (B), immunostained for γ-H2AX
758 (D) or pATM (E) (*SI Appendix,* Fig. S5*F-G*) and quantified as indicated. In both experiments, cells were
759 transfected with vectors expressing either untagged or 3×FLAG-IE1. *(F)* Representative images of pATM
760 inhibition at the mCherry-LacRnls-NBS1 locus. Cells were treated as described in (B). Representative images
761 of the negative controls are presented in *SI Appendix,* Fig. S5*G-H*. *(G)* Representative images of NBS1-

762 dependent IE1 recruitment to DSBs. Cells were treated with a siCTRL or siNBS1 prior to their transfection with
763 an untagged IE1 or an empty vector. ER-mCherry-LacR-FOKI-DD was induced as described in (B). Cells were
764 processed for IE1 immunofluorescence. *(H)* Quantification of the mCherry-LacR FOKI foci colocalizing with IE1.
765 Data represent the mean ± SD (n = 3). **p < 0.05, **p < 0.01, *** p<0.001, ****p < 0.0001. Scale bars = 5 µm.
766

767 **Fig. 6.** IE1 interacts with NBS1 and inhibits ATM through two distinct domains *(A)* Schematic of HHV-6B IE1
768 and the protein fragments used in this study. NBS1-BD, NBS1-binding domain; NBS1i, NBS1 inhibitory domain,
769 STAT2-BD: STAT2 binding-domain (aa 270–540). *(B-C)* U2OS 2-6-5 cells transfected with plasmids expressing
770 the indicated mCherry-LacR fusion proteins were immunostained for NBS1 (see also *SI Appendix,* Fig. S6*A-B*).
771 The mCherry-LacR backbone was used as a negative control (--). *(D-E)* Quantification of cells with > 10 γ-H2AX
772 foci. UT, untreated. Transiently transfected cells were irradiated and immunostained for γ-H2AX 1 h later (see
773 also *SI Appendix,* Fig. S6*G*). Untreated cells and the mCherry-LacR backbone were used as negative controls
774 (--). *(F)* Schematic of NBS1 and the protein fragments used in this study. FHA, forkhead-associated domain;
775 BRCT, BRCA1 C-terminal domain; MRE11-BM, MRE11-binding motif; ATM-BM, ATM-binding motif; IDD,
776 intrinsically disordered domain. *(G-H)* U2OS 2-6-5 cells were transfected with the indicated mCherry-LacR
777 plasmids and immunostained for IE1 (*SI Appendix,* Fig. S6*H-M*). *(I)* U2OS cells treated with siCTRL or siNBS1
778 were transfected with the indicated 3×FLAG and mCherry-LacR constructs. After 24 h, WCEs were prepared
779 and 3×-FLAG-IE1 interactors were immunoprecipitated using anti-Flag (M2) agarose beads and immunoblotted
780 for FLAG, mCherry, and NBS1. β-tubulin (Tub.) was used as a loading control. Data for *(B), (D),* and *(G)*
781 represent the mean ± SD (n = 3). ** p<0.01, ****p < 0.0001. Scale bars = 5 µm.
782

783 **Fig. 7.** NBS1 depletion impairs viral integration in cells maintaining their telomeres by homology-directed repair
784 *(A)* HHV-6B infection in permissive and semi-permissive cells. In cells semi-permissive for HHV-6B, replication
785 is inefficient, and the viral genome integrates at the telomeres. *(B)* MOLT-3 cells with and without NBS1 (*SI*
786 *Appendix,* Fig. S7*A*) were infected with HHV-6B at a MOI of 1 and harvested at the indicated time points.
787 Following cell lysis, DNA was extracted and HHV-6B was quantified by qPCR using primers for HHV-6B *U67-*
788 *68* and human *RPP30*. Data represent the mean ± SD (n = 3). *(C)* MOLT-3 cells were transduced with the
789 indicated shRNA and passaged 5 times prior to CellTiter-Glo® analyses. Cell viability was determined using
790 standard curves for each cell line and normalized to the shCTRL condition for each experiment.

Table 1. Importance of NBS1 for HHV-6B chromosomal integration in ALT$^{+/-}$ cells

Cell line	ALT status	shRNA	% cells with integrated HHV-6B[a] (n)[b]	*P* value[c]
HeLa	Negative	CTRL	0.96 (36,320)	$<2.2e^{-16}$
		NBS1	6.11 (33,280)	
GM847	Positive	CTRL	0.65 (21,820)	$<2.2e^{-16}$
		NBS1	0.01 (18,320)	
U2OS	Positive	CTRL	1.60 (20,000)	$<2.2e^{-16}$
		NBS1	0.69 (21,520)	
U2OS *PML*$^{-/-}$	Positive	CTRL	0.71 (28,220)	ns[d]
		NBS1	0.78 (30,460)	

[a] mean of three independent cultures

[b] total number of cells analyzed

[c] Pearson's Chi-squared test with Yates' continuity correction

[d] ns, not significant

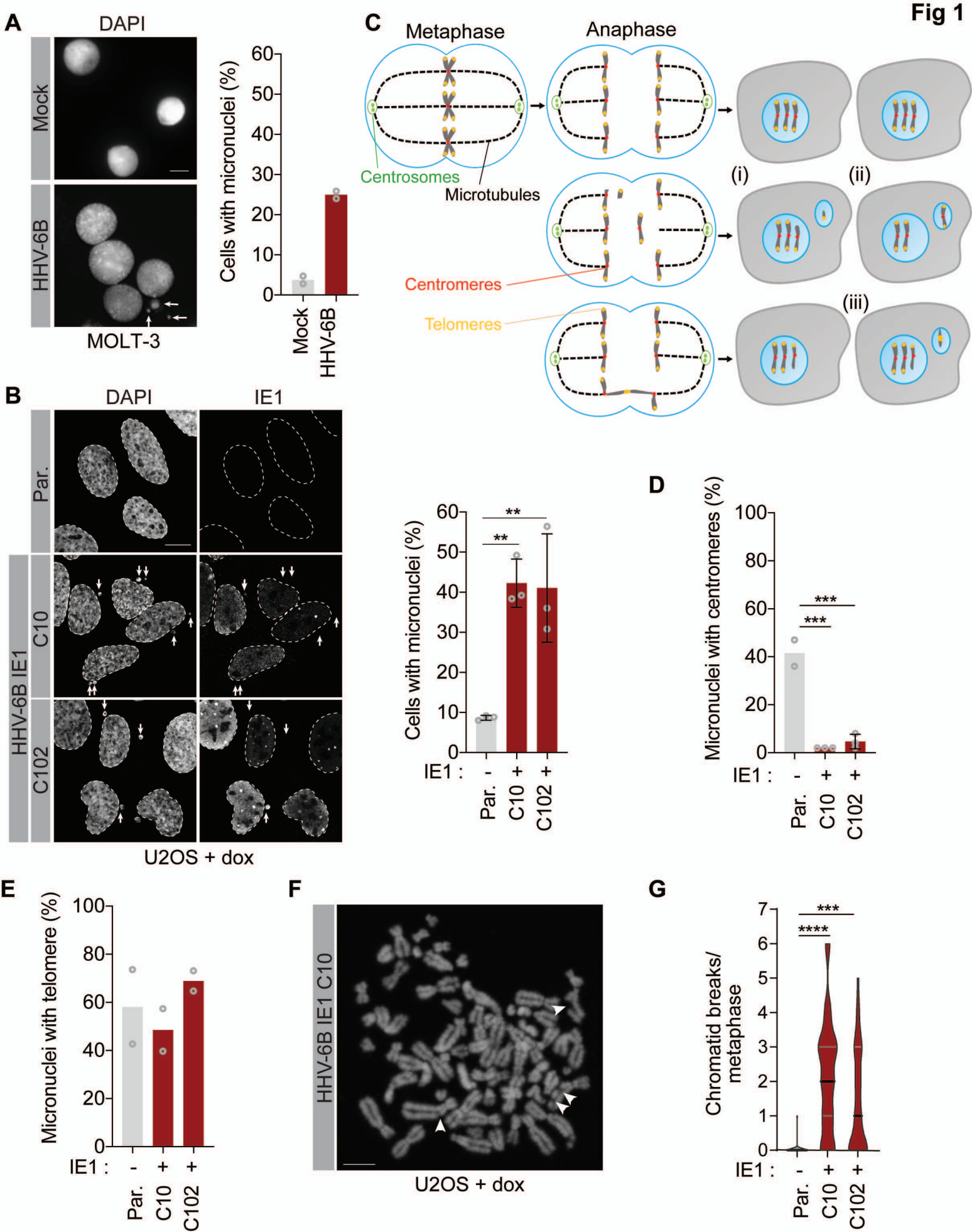
Fig 1
A
DAPI
Mock
HHV-6B
MOLT-3
Cells with micronuclei (%)
60
50
40
30
20
10
0
Mock
HHV-6B
C
Metaphase
Anaphase
Centrosomes
Microtubules
Centromeres
Telomeres
(i)
(ii)
(iii)
B
DAPI
IE1
Par.
HHV-6B IE1
C10
C102
U2OS + dox
Cells with micronuclei (%)
**
**
IE1 :
-
+
+
Par.
C10
C102
D
Micronuclei with centromeres (%)
100
80
60
40
20
0
***
***
IE1 :
-
+
+
Par.
C10
C102
E
Micronuclei with telomere (%)
100
80
60
40
20
0
IE1 :
-
+
+
Par.
C10
C102
F
HHV-6B IE1 C10
U2OS + dox
G
Chromatid breaks/ metaphase
7
6
5
4
3
2
1
0
***
****
IE1 :
-
+
+
Par.
C10
C102

Fig.2

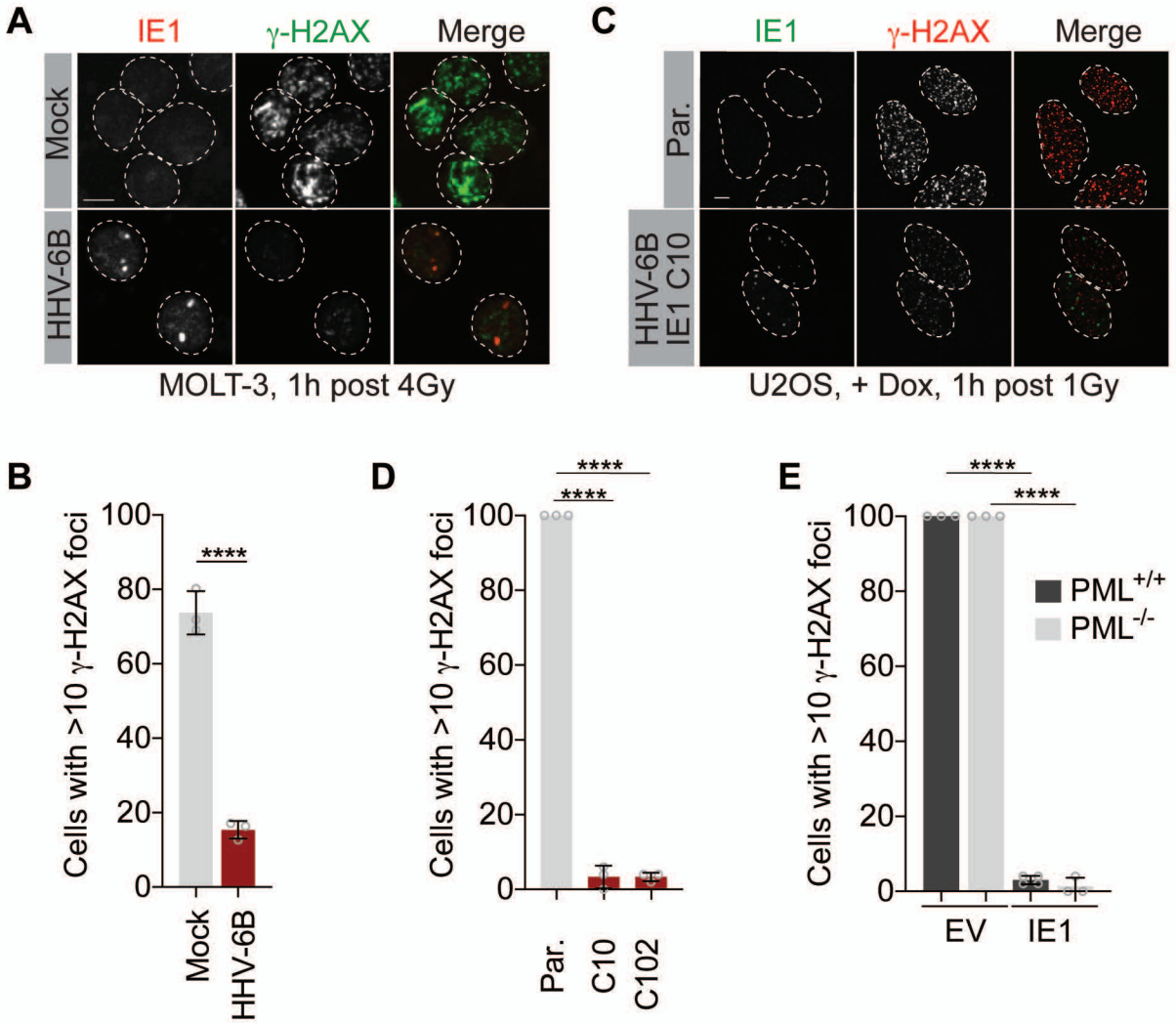
A
IE1
γ-H2AX
Merge
Mock
HHV-6B
MOLT-3, 1h post 4Gy
C
IE1
γ-H2AX
Merge
Par.
HHV-6B IE1 C10
U2OS, + Dox, 1h post 1Gy
B
Cells with >10 γ-H2AX foci
100
80
60
40
20
0
****
Mock
HHV-6B
D
Cells with >10 γ-H2AX foci
****
****
Par.
C10
C102
E
Cells with >10 γ-H2AX foci
****
****
PML+/+
PML-/-
EV
IE1

Fig.3

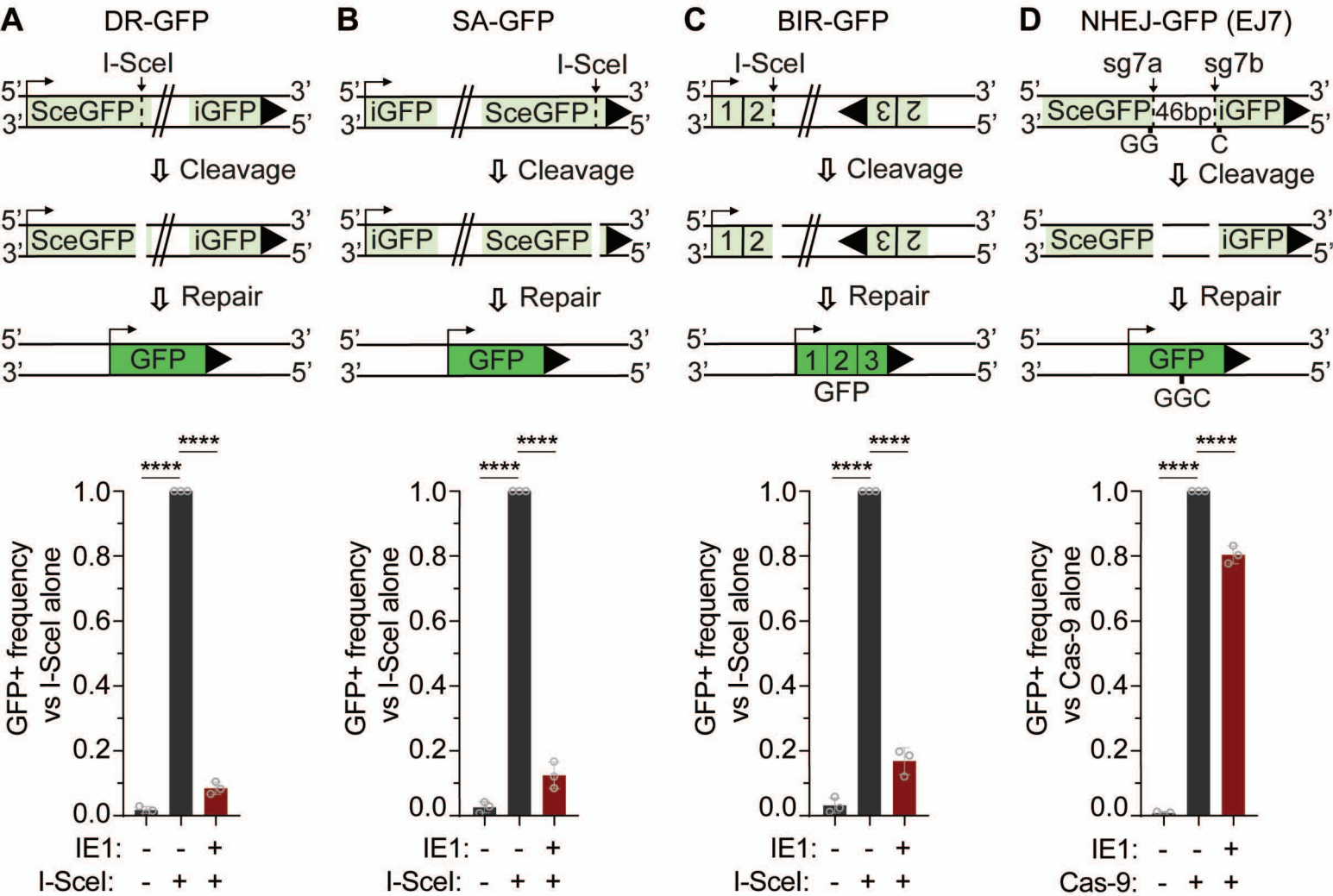
A
DR-GFP
I-SceI
SceGFP
iGFP
Cleavage
Repair
GFP
B
SA-GFP
I-SceI
iGFP
SceGFP
Cleavage
Repair
GFP
C
BIR-GFP
I-SceI
1
2
3
Cleavage
Repair
GFP
D
NHEJ-GFP (EJ7)
sg7a
sg7b
SceGFP
46bp
iGFP
GG
C
Cleavage
Repair
GFP
GGC
5'
3'
GFP+ frequency vs I-SceI alone
GFP+ frequency vs Cas-9 alone
****
IE1:
I-SceI:
Cas-9:

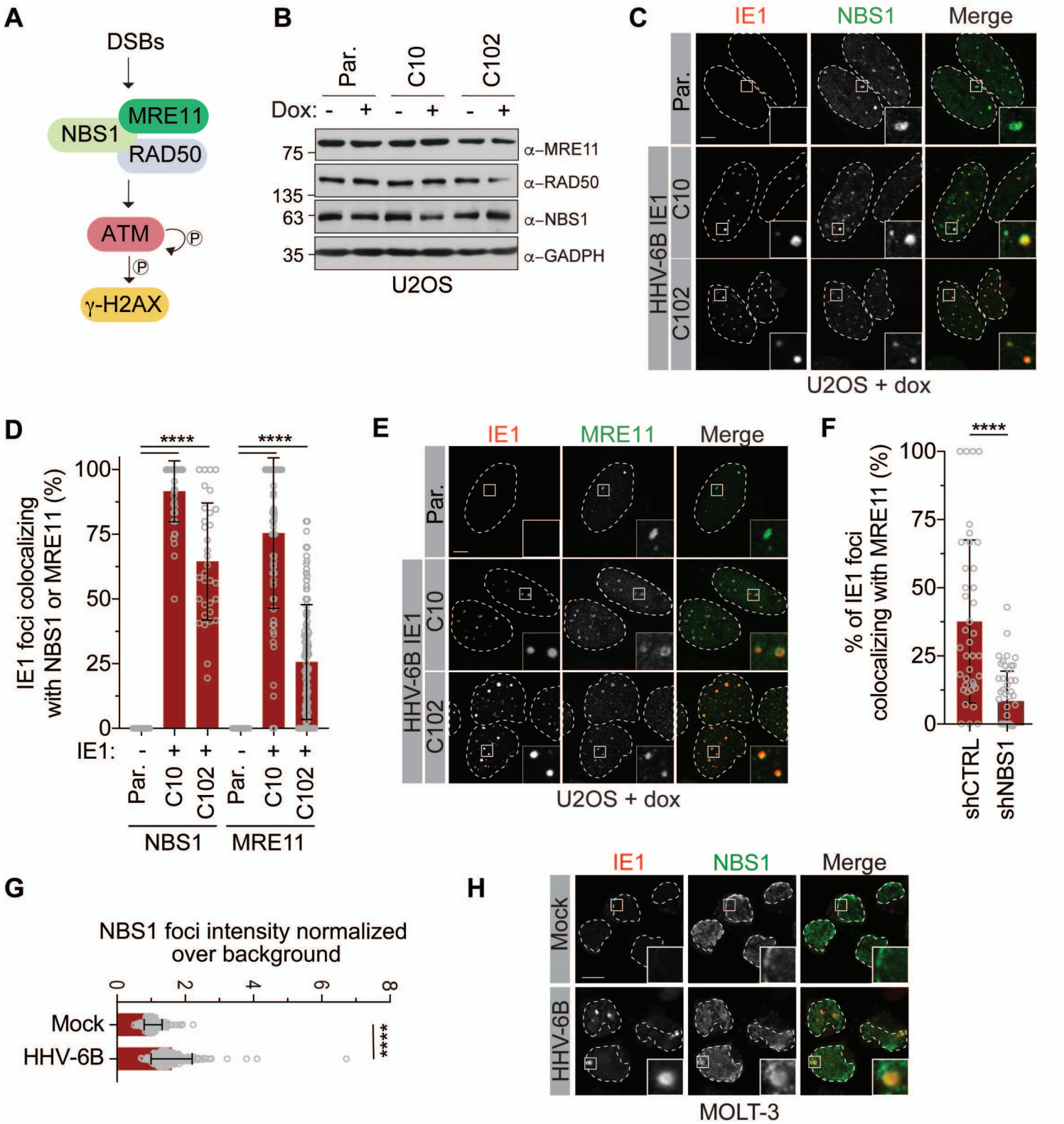
A
DSBs
MRE11
NBS1
RAD50
ATM
P
P
γ-H2AX
B
Par.
C10
C102
Dox: - + - + - +
75
135
63
35
α–MRE11
α–RAD50
α–NBS1
α–GADPH
U2OS
C
IE1
NBS1
Merge
Par.
HHV-6B IE1
C10
C102
U2OS + dox
D
IE1 foci colocalizing with NBS1 or MRE11 (%)
****
****
100
75
50
25
0
IE1: - + + - + +
Par.
C10
C102
Par.
C10
C102
NBS1
MRE11
E
IE1
MRE11
Merge
Par.
HHV-6B IE1
C10
C102
U2OS + dox
F
% of IE1 foci colocalizing with MRE11 (%)
****
100
75
50
25
0
shCTRL
shNBS1
G
NBS1 foci intensity normalized over background
0
2
4
6
8
Mock
HHV-6B
****
H
IE1
NBS1
Merge
Mock
HHV-6B
MOLT-3

Fig. 5

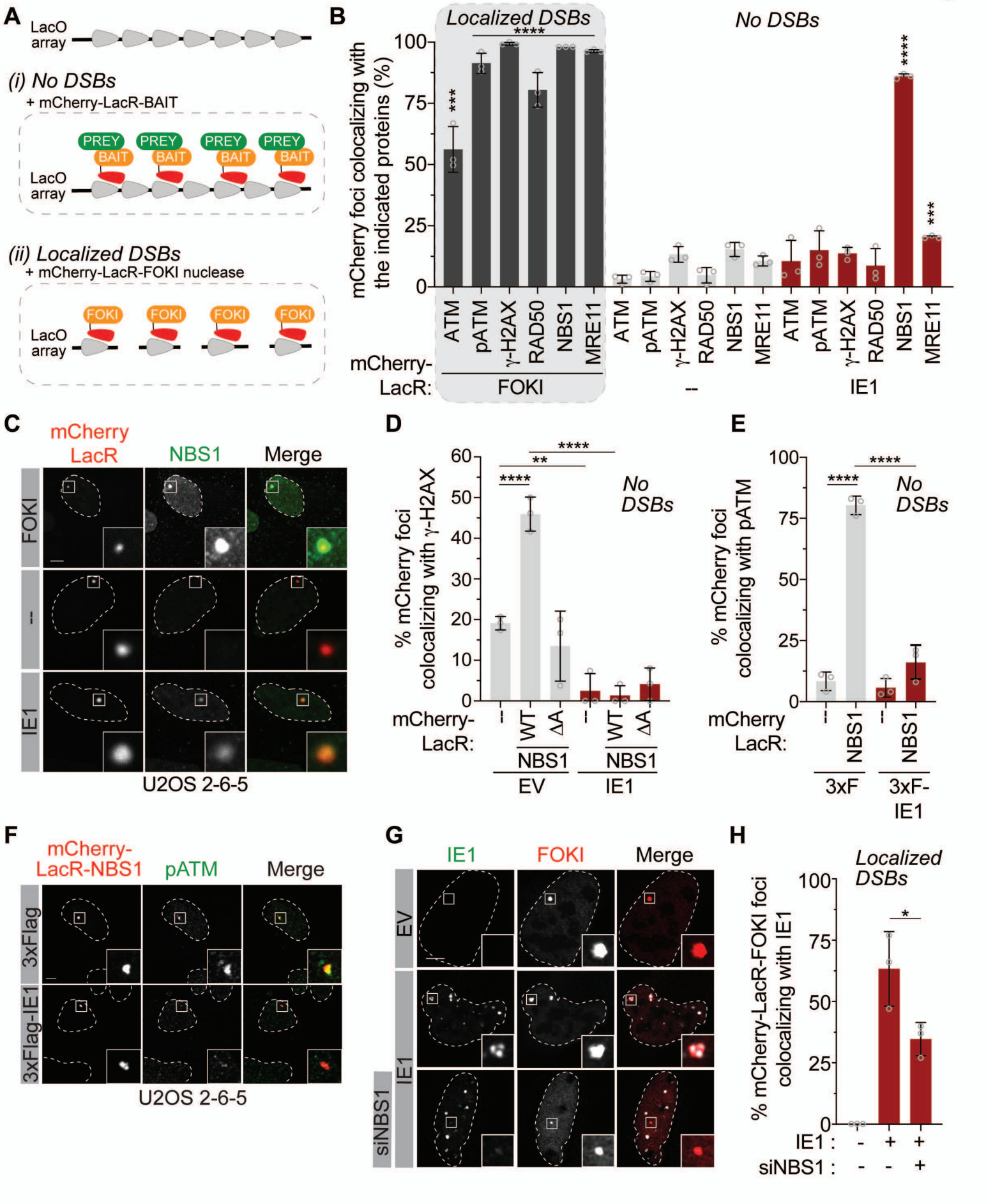
A
LacO array
(i) No DSBs
+ mCherry-LacR-BAIT
PREY
BAIT
LacO array
(ii) Localized DSBs
+ mCherry-LacR-FOKI nuclease
FOKI
LacO array
B
Localized DSBs
No DSBs
mCherry foci colocalizing with the indicated proteins (%)
ATM
pATM
γ-H2AX
RAD50
NBS1
MRE11
mCherry-LacR:
FOKI
--
IE1
C
mCherry LacR
NBS1
Merge
FOKI
--
IE1
U2OS 2-6-5
D
% mCherry foci colocalizing with γ-H2AX
No DSBs
mCherry-LacR:
WT
ΔA
NBS1
EV
IE1
E
% mCherry foci colocalizing with pATM
No DSBs
mCherry LacR:
NBS1
3xF
3xF-IE1
F
mCherry-LacR-NBS1
pATM
Merge
3xFlag
3xFlag-IE1
U2OS 2-6-5
G
IE1
FOKI
Merge
EV
IE1
siNBS1
H
Localized DSBs
% mCherry-LacR-FOKI foci colocalizing with IE1
IE1 :
siNBS1 :

Fig 6

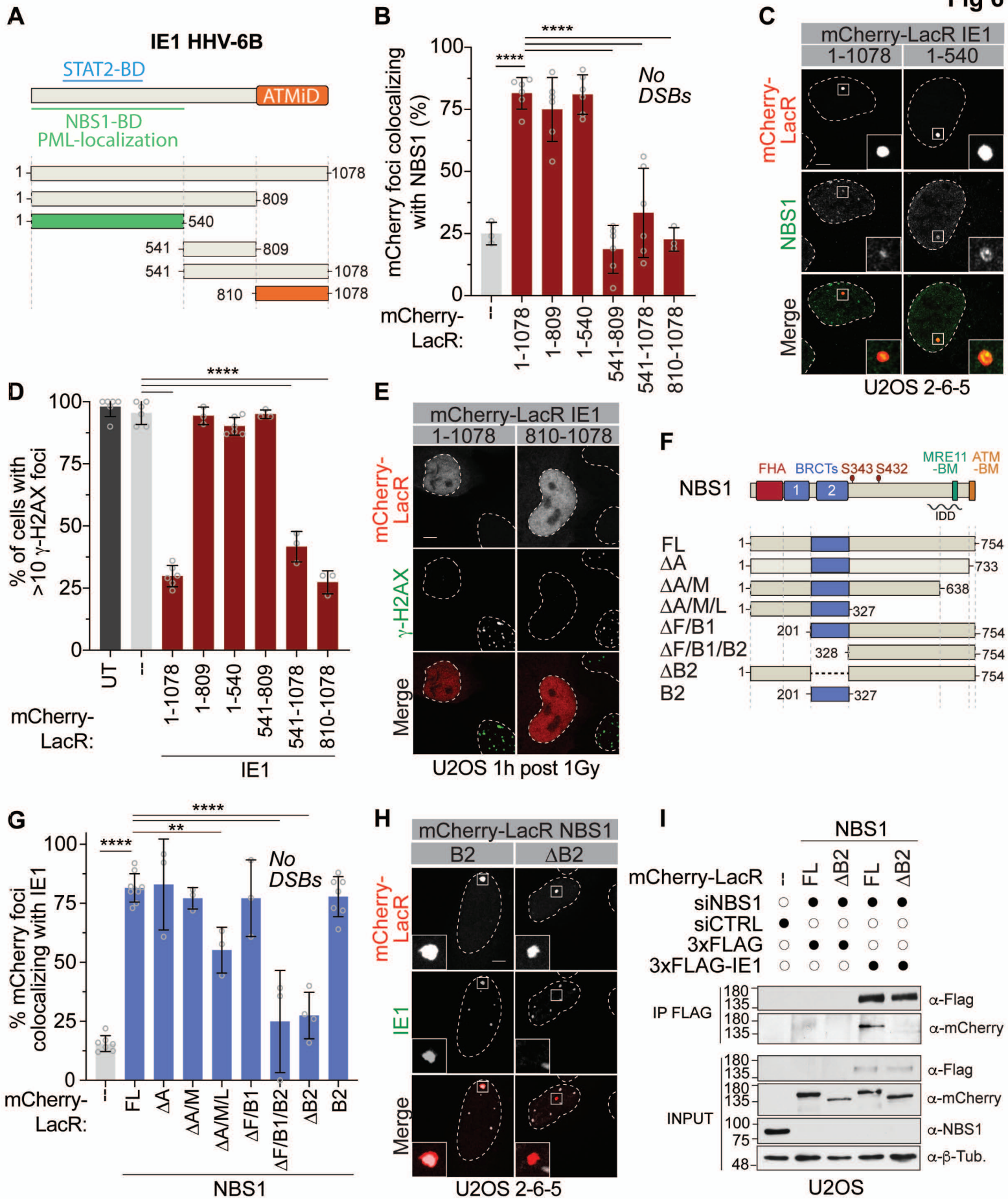
A
IE1 HHV-6B
STAT2-BD
ATMiD
NBS1-BD
PML-localization
1
1078
809
540
541
810
B
mCherry foci colocalizing with NBS1 (%)
No DSBs
****
mCherry-LacR:
-
1-1078
1-809
1-540
541-809
541-1078
810-1078
C
mCherry-LacR IE1
1-1078
1-540
mCherry-LacR
NBS1
Merge
U2OS 2-6-5
D
% of cells with >10 γ-H2AX foci
UT
IE1
E
mCherry-LacR IE1
1-1078
810-1078
γ-H2AX
U2OS 1h post 1Gy
F
NBS1
FHA
BRCTs
S343
S432
MRE11 -BM
ATM -BM
IDD
FL
ΔA
ΔA/M
ΔA/M/L
ΔF/B1
ΔF/B1/B2
ΔB2
B2
754
733
638
327
201
328
G
% mCherry foci colocalizing with IE1
ΔF/B1/B2
ΔB2
B2
NBS1
H
mCherry-LacR NBS1
B2
ΔB2
IE1
U2OS 2-6-5
I
NBS1
siNBS1
siCTRL
3xFLAG
3xFLAG-IE1
IP FLAG
INPUT
α-Flag
α-mCherry
α-NBS1
α-β-Tub.
U2OS

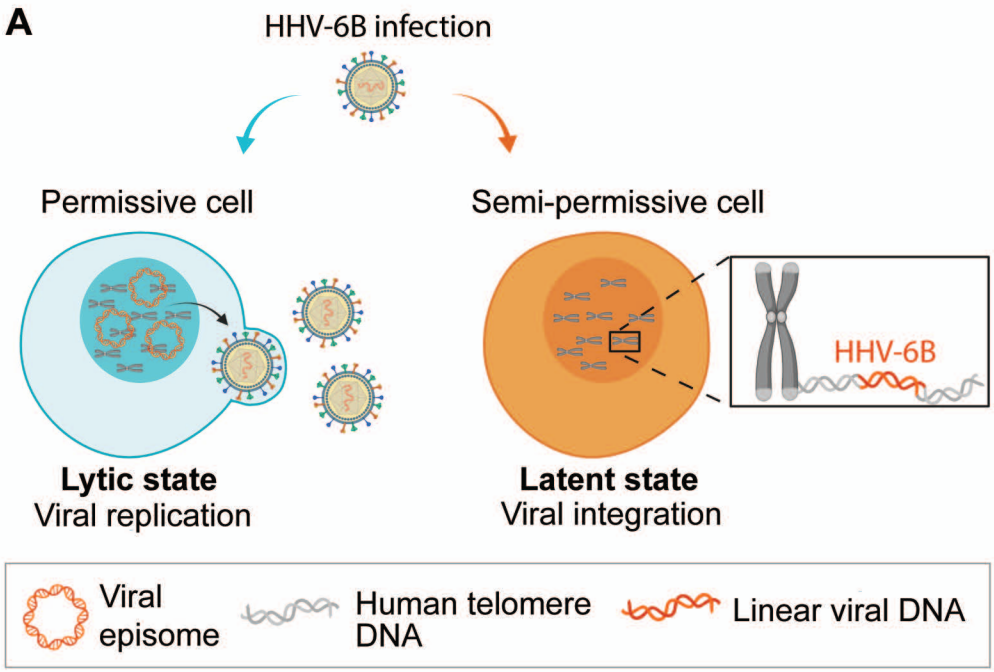
A
HHV-6B infection
Permissive cell
Semi-permissive cell
HHV-6B
Lytic state
Viral replication
Latent state
Viral integration
Viral episome
Human telomere DNA
Linear viral DNA

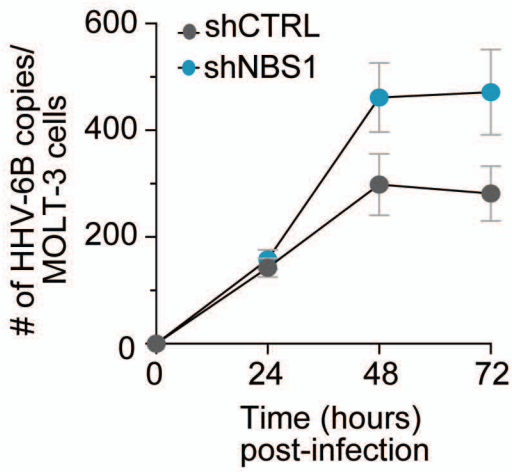
B
shCTRL
shNBS1
# of HHV-6B copies/ MOLT-3 cells
600
400
200
0
0
24
48
72
Time (hours) post-infection

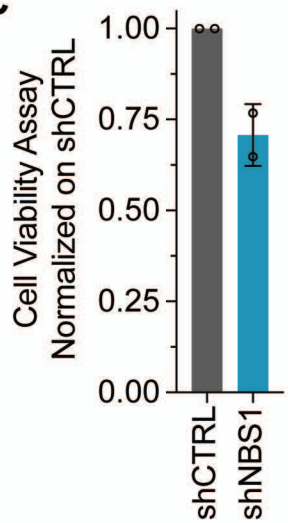
C
Cell Viability Assay Normalized on shCTRL
1.00
0.75
0.50
0.25
0.00
shCTRL
shNBS1